PCCP
Physical Chemistry Chemical Physics

Accepted Manuscript

This article can be cited before page numbers have been issued, to do this please use: A. M. Belenguer, *Phys. Chem. Chem. Phys.*, 2026, DOI: 10.1039/D6CP00448B.

ROYAL SOCIETY OF CHEMISTRY

rsc.li/pccp

View Article Online
DOI: 10.1039/D6CP00448B

ARTICLE

Unravelling Key Phenomena in Ball Milling Reactions Toward Fundamental Principles-— A Minireview Tutorial

Ana M. Belenguer

Received 00th January 20xx,
Accepted 00th January 20xx

DOI: 10.1039/x0xx00000x

Mechanochemistry is an emerging solvent-free approach in which chemical and supramolecular processes are driven by mechanical forces acting on solid reagents. In particular ball milling, a central approach within mechanochemistry, can generate nanoscale domains and activate reactivity through mechanical energy, offering a green and energy-efficient alternative to conventional solution -based methods. Unlike solution chemistry—whose principles are well established—the mechanisms underlying ball milling processes remain under active investigation. Ball milling reactions obey the same thermodynamic principles and underlying molecular mechanisms as solution-based reactions; however, the dominant energy inputs differ significantly. In ball milling, energy is delivered locally and intermittently through mechanical impacts rather than uniformly via thermal activation. Combined with the absence of solvent, the presence of lattice defects, and solid-state constraints, these factors can substantially alter reaction kinetics, accessible pathways, and product distributions. The purpose of this minireview -tutorial is to present, from my perspective, the contributions of my collaborators and myself toward understanding the unique phenomena associated with ball milling. We hope these insights will help advance the establishment of the fundamental principles of ball milling. .

1 Introduction

Most organic reactions in academic and industrial laboratories continue to rely on solvothermal activation, in which heat and large volumes of solvent are used to drive chemical transformations. The solvent waste and energy demands associated with such processes are increasingly recognised as environmentally and economically unsustainable. Consequently, there is an urgent need for alternative activation strategies that reduce waste and energy consumption while maintaining or improving reaction efficiency and selectivity.

In this context, ball milling, a central approach within mechanochemistry, which uses mechanical energy to promote chemical and supramolecular transformations in the solid state, has emerged as a powerful and sustainable alternative to solution-based synthesis. By operating without bulk solvents and often without external heating, ball mill reactions can exhibit enhanced efficiency and selectivity, arising in part from the close and regular arrangement of molecules within crystalline solids.[1-3]

The earliest mechanochemical phenomena were observed by Michael Faraday, who in 1820 reported that grinding silver chloride with Zn, Cu, Sn, or Fe in a mortar and pestle induced its reduction—a process he described as the “dry way” of effecting chemical reactions.[4] Systematic investigations followed in the late nineteenth century through the work of M. Carey Lea, widely regarded as the father of mechanochemistry. M. Carey Lea demonstrated that mechanical force could induce chemical transformations comparable to, and in some cases more effective than, thermal activation. Crucially, he showed that mechanochemistry enables reactivity inaccessible under purely thermal conditions: for example, while mercuric chloride sublimes and silver chloride melts upon heating without decomposition, both compounds readily decompose under mechanical grinding. The term mechanochemistry was formally introduced in 1919, when Wilhelm Ostwald classified it as one of four fundamental sub-disciplines of chemistry—alongside thermochemistry, electrochemistry, and photochemistry—each defined by a distinct mode of energy input. A comprehensive historical account has been provided by Takacs.[4]

Despite these early insights, mechanochemistry remained largely confined to insoluble inorganic materials, such as alloys and metal oxides, throughout much of the mid-twentieth century, often employed only when no viable solvent-based alternative existed.[4] Renewed interest in mechanochemical methods, particularly ball milling, has been driven by growing sustainability concerns and by the recognition of their unique reactivity profiles.

Ball milling reactions are typically performed under stoichiometric conditions, making them inherently atom economic. They often proceed under mild conditions, without external heating, and with little or no solvent, offering substantial environmental and energy advantages. Life-cycle assessments indicate that the environmental impact and cost of ball milling processes can be reduced by orders of magnitude compared with conventional solution-based routes.[5, 6] These benefits are commonly attributed to particle size reduction,

[a] Yusuf Hamied Department of Chemistry, University of Cambridge, Lensfield Road, Cambridge CB2 1EW, UK.
† email: amb84@cam.ac.uk

View Article Online
DOI: 10.1039/D6CP00144B

increased surface area, enhanced contact between reactants, minimised mass-transfer limitations, and accelerated reaction rates. X-ray diffraction studies further reveal that mechanical activation induces the accumulation of lattice defects and, in some cases, amorphization, providing a microscopic basis for the observed reactivity enhancements.[4] Different types of ball milling transformation have been considered.[7]

A comprehensive comparative analysis by Reynes et al. in 2024 systematically evaluated reactions performed by ball milling against their solution-phase analogues, with a particular focus on main-group inorganic chemistry (Groups 1, 2, 13, and 14).[8] These reactions, which are often conducted under inert atmospheres, were shown to be reproducible under mechanochemical conditions and, in most cases, proceeded with shorter reaction times, higher yields, and milder conditions—typically at room temperature—while avoiding toxic solvents and expensive catalysts.[8] Notably, several examples involving transition-metal chemistry were also demonstrated to be feasible under air, with ball-milled reactions occurring more rapidly and affording higher yields than their solution-based counterparts.[8] Similarly, organic mechanosynthesis can often be conducted under ambient conditions, delivering products in shorter times and with improved yields. The same review highlighted that numerous metal–organic frameworks (MOFs) and perovskite materials can be readily synthesised mechanochemically under air, whereas analogous solution-based preparations have not been reported.[8] Consistent with these findings, Andersen and Starbuck observed significant rate and yield enhancements for nucleophilic aromatic substitution reactions under ball milling conditions relative to solution-phase protocols.[9]

In several notable cases, ball milling enables reactivity that has no solution-phase analogue. Examples of such unique behaviour have been reported across inorganic[8] and organic chemistry[8, 10] Curtin and Paul demonstrated that a simple mortar-and-pestle approach allowed the preparation by mechanochemistry of unsymmetrical substituted quinhydrones that are too unstable toward oxidation to be synthesised in solution.[11] Ball milling has been shown to induce the formation of a previously inaccessible η-chlorpropamide (CPA) polymorph[12, 13] and to enable recovery of Form I of the "disappearing polymorph" of ritonavir.[14]

The transformative potential of mechanochemistry was formally recognised in 2019, when the International Union of Pure and Applied Chemistry (IUPAC) identified it as one of the top ten emerging technologies in chemistry with the capacity to "change the world".[15] This recognition reflects the remarkable breadth of contemporary ball milling research, as documented in recent reviews spanning organic synthesis,[8, 16] inorganic transformations,[17] metal–organic frameworks (MOFs) and covalent organic frameworks (COFs),[18] luminescent coordination polymers[19], polymer synthesis,[20] polymer degradation,[21] cocrystal formation,[22, 23] supramolecular and macrocyclic chemistry,[24] environmental applications such as waste upcycling,[25] and mineral processing.[26]

As the field has expanded, efforts have been made to organise ball mill knowledge and facilitate its broader adoption. A concise primer on ball milling was published in 2025,[27] while organic mechanochemical reactions have been systematically catalogued according to the types of bonds formed, providing a practical framework for identifying relevant precedents.[28] Comprehensive reviews have also addressed the historical development, nomenclature, instrumentation, and leading contributors to the field,[29] alongside emerging insights into the thermodynamics and kinetics of mechanochemical including ball milling processes[30] and detailed mechanistic studies of ball-milling reactions.[2, 31]

The enormous range of applications for ball milling synthesis implies an equally diverse set of governing transformation processes, lending a certain refinement to this complexity. Mechanical force not only alters molecular geometry but also perturbs intermolecular noncovalent interactions, leading to changes in crystal packing and polymorphism. By manipulating crystal packing, mechanical force provides a means to modify bulk physical properties such as lattice stability, melting temperature, and compressibility.[29] Consequently, while many elementary steps characteristic of solution-phase reactions may still apply to ball milling systems, additional elementary processes must be considered to fully describe their reaction mechanisms.[29]

Significant progress has been made toward understanding the fundamental mechanisms underlying these transformations. The prevailing kinetic theory of ball milling proposes that grinding induces particle comminution to submicron or nanoscale crystallites, dramatically increasing surface area and the probability of reactive collisions.[2] X-ray diffraction studies further suggest that the primary microscopic effect of mechanical treatment is the accumulation of lattice defects.[32] Mechanical activation thus stores energy within the solid in the form of defects or other structural modifications, lowering activation barriers or improving steric accessibility for subsequent reactions. Typically, mechanical activation leads to either polymorphic transitions or amorphization. However, the precise mechanism remains unresolved, particularly whether these transformations arise from the gradual accumulation of extended defects or proceed via contact melting followed by recrystallization.[32]

Although ball milling offers numerous advantages and has demonstrated applicability across diverse areas of chemistry, its adoption in chemical synthesis and industrial manufacturing remains limited. This limited uptake is largely attributed to persistent gaps in the fundamental understanding of ball milling reactivity. The mechanisms by which reactions are initiated and propagated under mechanical force, as well as the underlying driving forces of these processes, remain incompletely understood. A deeper mechanistic understanding is therefore considered essential for rationalising experimental observations and enabling the rational design of ball milling processes.

Mechanistic elucidation is rarely defined as an explicit objective in ball milling studies; instead, most investigations prioritize the preparation of materials with targeted properties or the optimization of processes to meet specific performance criteria. In addition, difficulties in scaling ball milling methods from

View Article Online
DOI: 10.1039/D6CP00448B

laboratory to industrial contexts, along with limited interlaboratory reproducibility, continue to hinder broader adoption.

The acceptance of the topic of mechanochemistry is further constrained by its limited inclusion in undergraduate curricula, which trains chemists predominantly within the framework of solution-based reactivity. Shifting from this established paradigm to the fundamentally different, non-solution-based logic of mechanochemistry requires a substantial conceptual adjustment.

As illustrated in Figure 1, the properties of crystalline starting materials and products must therefore be regarded as key determinants of ball milling reactions and transformations. Figure 1 illustrates the base-catalysed disulfide exchange between the two homodimers, bis(2-nitrophenyl) disulfide (1–1) and bis(4-chlorophenyl) disulfide (2–2), in the presence of 1,8-diazabicyclo[5.4.0]undec-7-ene (DBU), to yield the heterodimer 2-nitrophenyl-4-chlorophenyl disulfide (1–2). Depending on the milling conditions, the heterodimer can be obtained in two distinct polymorphic forms. Neat ball milling affords Form A, as shown in Figure 1b and Figure 6a, whereas the addition of a few drops of solvent to the powder leads to the formation of Form B, as discussed later and shown in Figure 6b.

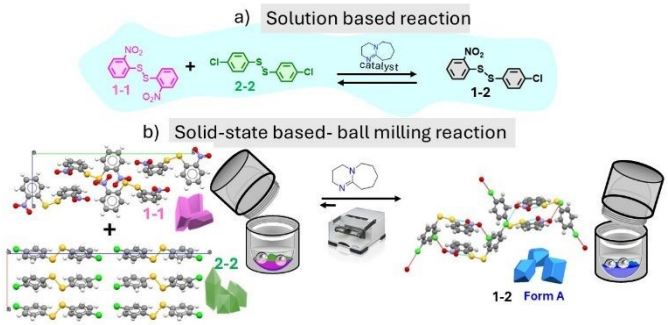

Figure 1 Visual conception of a disulfide exchange reaction scheme under a) solution-based conditions using molecular structures of the homodimers (1-1, 2-2) and the heterodimer (1-2) dissolved in a solvent (in light blue); b) under ball milling conditions depicting the crystal structures of the starting materials (1-1 and 2-2) and products involved (Form A polymorph of 1-2).

2 Ball milling reactors

Mechanochemical methods involve chemical transformations induced by mechanical energy, such as compression, shear, or friction, and are most implemented using techniques such as ball milling. While manual grinding is subject to variable human and environmental influences, modern milling technologies—including ball mill shaker and planetary mills—provide enclosed and controlled environments that enable more consistent and reproducible results.[8, 18, 29] The mechanochemical community quickly recognised the utility of commercially available milling equipment (Figure 2) and jars (Figure 3) for conducting solid-state reactions and has relied on these systems extensively.

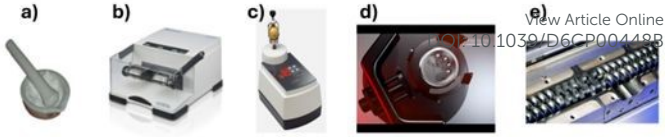

Figure 2 Milling equipment used in mechanochemistry: a) manual mortar and pestle; b) and c) vibratory ball milling equipment exerting b) horizontal movement through a shallow pendular arch; c) vertical movement; d) planetary equipment and e) twin screw extruder.

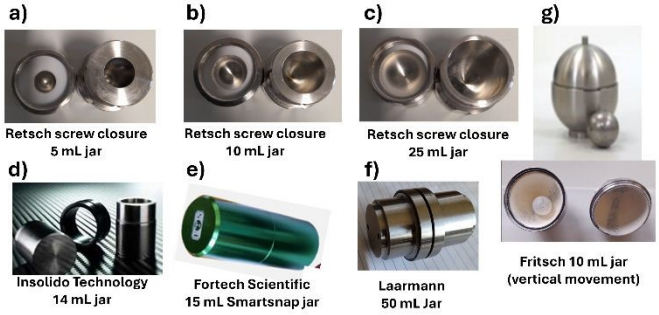

Figure 3 Commercially available jars used for vibrational ball milling. The internal shape of the top and bottom caps are hemispheres, connected through a cylindric section. a) to f) used under horizonal vibratory motion using ball mills depicted in Figure 2b). The milling jar in g) is used for vertical motion using ball mills depicted in Figure 2c).

However, caution is warranted when applying the operational guidelines provided by equipment manufacturers. Recommendations concerning powder loading, ball size and number, and milling duration are generally optimised for mechanical processing or particle-size reduction, rather than for promoting controlled chemical transformations. Consequently, these guidelines are not always directly transferable to studies focused on ball milling reactivity and may require careful adaptation to ensure reproducible and selective outcomes.

3 Neat grinding and liquid assisted grinding.

Ball milling reactions are commonly categorised using liquid additives. Neat grinding (NG; Figure 4a) proceeds without any added liquid, while liquid-assisted grinding (LAG; Figure 4b) introduces a sub-stoichiometric amount to modulate reactivity.

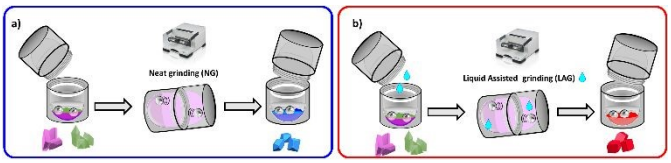

Figure 4. Milling of two crystalline starting materials (pink and green): (a) under neat grinding (NG) conditions, in the absence of added solvent, yields a distinct crystalline product polymorph (blue); (b) under liquid-assisted grinding (LAG) conditions, in the presence of a sub-stoichiometric amount of solvent, produces a different crystalline product polymorph (red)

A landmark study by Karki et al. (2007) demonstrated that both NG and LAG are significantly more efficient than conventional solution-based crystallization methods for cocrystal screening and synthesis.[33]

LAG promotes chemical reactivity and solid-state transformations through the addition of small amounts of liquid—typically a few microliters per milligram of solid—which

View Article Online
DOI: 10.1039/D6CP00448B

can control reaction rates, product selectivity, and reaction pathways. Such additives are capable of modulating reactivity, directing supramolecular assembly, and, in some cases, altering the chemical nature of mechanochemical products.[34]

The earliest documented use of a liquid additive in a mechanochemical reaction dates to the fourth century B.C., when cinnabar (HgS) was ground with vinegar to release elemental mercury. In this rudimentary process, the liquid (vinegar) presumably acted as a lubricant, facilitating particle contact and accelerating reactivity.[4]

The historical development of NG and LAG in mechanochemistry was comprehensively reviewed in 2012,[1] while a focused review on cocrystal formation appeared in 2013.[35]

Beyond NG and LAG, other mechanochemical approaches utilise solid additives or viscous liquids. Ion-and-liquid assisted grinding (ILAG) employs ion additives such as $NaNO_3$, NH_4Cl, or NH_4NO_3, often in combination with small amounts of solvent.[36] In polymer-assisted grinding (PoLAG), short- or long-chain polymers, such as polyethylene glycols, serve as additives.[37] A recent review covers all aspect of NG, LAG and ILAG for the preparation of polymorphs, cocrystals, salts, MOFs and synthesis of organic compound.[38]

4 Preparation of ball milling reactions

Accurate stoichiometry is essential in mechanochemical reactions. Starting materials should be weighed precisely prior to transfer into the milling jar to ensure the correct stoichiometric ratio. Inaccurate weighing can lead to residual excess reactants in the final product, negatively impacting yield and purity. Subsequent steps in the mechanochemical procedure are generally tolerant of minor variations, as demonstrated in video clips published in the Journal of Visualized Experiments (JoVE). The overall procedure is illustrated schematically in Figure 5.[39]

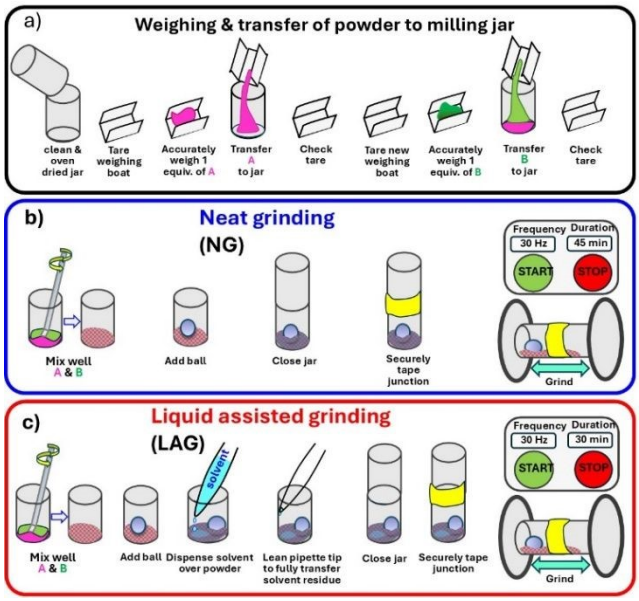

Figure 5: Protocol steps for the execution of ball mill reactions. a) Weighing and careful transfer of powder of the 2 starting materials (A and B) to the milling jar; b) and c) indicates the steps required to perform NG and LAG reactions. This procedure has been published as video clips in a visual form.[39]

5 Opportunity to unravel fundamental principles of ball milling reactions

In 2010, Tomislav Friščić joined the Department of Chemistry at the University of Cambridge and encouraged Professor Jeremy Sanders and me—both working in dynamic covalent chemistry (DCC) in solution,[40] to explore ball milling. He argued that ball milling could offer faster and cleaner reactions with higher yields than conventional solution-based methods making them more sustainable. Professor Sanders is a pioneer of DCC, a field that traditionally relies on combining monomers in solution at millimolar or micromolar concentrations to generate dynamic covalent libraries.[40]

To test this claim, we selected a simple disulfide exchange reaction in which two homodimers interconvert to form a heterodimer. In solution, this exchange is known to yield a statistical mixture, limiting the heterodimer content to 50%.

In striking contrast, mechanochemical treatment afforded the heterodimer quantitatively in just 30 to 45 minutes. Solid-state analysis by powder X-ray diffraction further revealed that neat ball milling produced a distinct polymorph (Form A), whereas the addition of a few drops of MeCN led to a different polymorph (Form B).[41]

These results prompted a decisive shift in our research towards addressing fundamental gaps in the understanding of ball milling, a mechanochemical process that, at the time, lacked a coherent and predictive theoretical framework. Because fundamental principles must be universal, their validity should extend across chemical systems and disciplines.

In this minireview, we present a structured and critical analysis of the key trends uncovered by our multidisciplinary collaborative team in the field of ball milling. These trends have been systematically tested across diverse chemical systems with the explicit aim of evaluating their universality. Collectively, they establish a conceptual framework for rationalising ball milling reactivity and outcomes. Each trend constitutes an essential component of a broader mechanistic picture which, when integrated, advances the field towards a predictive understanding of ball milling processes. While ball milling remains an evolving discipline, the trends identified herein represent significant and generalisable progress beyond system-specific observations.

Our research efforts have focused on the following interconnected areas:

1) Driving forces governing ball milling reactions (Section 8)
2) Dynamic nature of ball milling reactions (Section 9)
3) Determinants of steady-state outcomes in ball milling reactions (Section 10)
4) Kinetic profiles of ball milling NG and LAG reactions, including unseeded systems and systems seeded with polymorphs of the reaction product (Section 11)
5) Role of crystal size reduction in ball milling reactivity (Section 12)

View Article Online
DOI: 10.1039/D6CP00448B

5) Polymorph formation, selection, and interconversion under ball milling conditions (Section 13)
6) Influence of the nature and volume of liquid additives in LAG reactions (Section 14)
7) Achieving homogeneity in ball milling reactions (Section 15)
8) Role of induction period in the kinetics of ball milling (Section 16)
9) Influence of milling frequency on steady-state composition (Section 18)
This minireview also discusses other research efforts (Section 17 and 19) not investigated by our multidisciplinary team which contributes to better understanding of ball milling.

6 Using model reactions to unravel trends in ball milling

Our experiments were designed to address key questions that, at the time, lacked clear answers. To this end, we selected two simple yet representative model reactions capable of providing reliable insights into the underlying mechanistic phenomena. These models serve as a foundation for understanding the dynamic behaviour of ball milling transformations and for extrapolating principles that may apply more broadly.

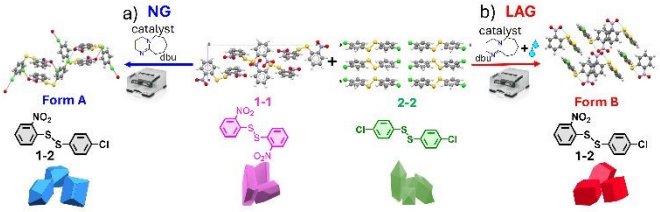

Figure 6 Model reaction used to probe ball milling trends. Base-catalysed (DBU) disulfide exchange between equimolar 1–1 and 2–2 yields the heterodimer 1–2. (a) Neat grinding (NG) produces polymorph Form A. (b) Liquid-assisted grinding (LAG) produces polymorph Form B.[41]

The primary model system is a simple base-catalysed disulfide exchange in which equimolar 1–1 and 2–2 react in the presence of DBU to form the heterodimer 1–2. This reaction involves the exchange of two disulfide homodimers to yield a heterodimer that exists in two polymorphic forms (Form A and Form B; Figure 6).
To extend this study, we investigated a cocrystal system. Cocrystals comprise two or more molecular or ionic components in a defined stoichiometric ratio and are neither solvates nor simple salts. Their crystal structures are governed by competing and cooperative noncovalent interactions, including hydrogen bonding, π–π stacking, and van der Waals forces.[22] We selected the 1:1 theophylline–benzamide (tp:ba) cocrystal, which exhibits two polymorphs (Form I and Form II; Figure 7). Previously reported by Emmerling et al.[42], this system served as a complementary model to test the generality of the trends observed in the disulfide exchange reaction.
Comparison of these two systems enabled us to assess how ball milling conditions influence polymorph selection across distinct classes of solid-state transformations.

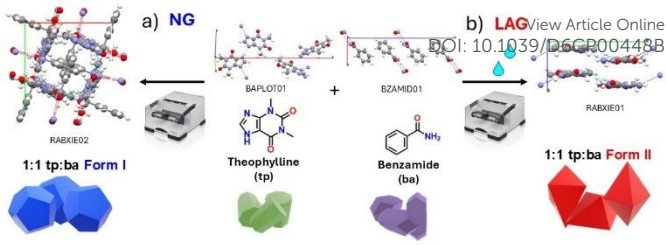

Figure 7: Selected cocrystal model reaction. 1:1 Theophylline: Benzamide cocrystal obtained from equimolar mixtures of theophylline anhydrous (tp) and benzamide (ba). a) Forming 1:1 tp:ba Form I (in blue) under NG conditions; b) 1:1 tp:ba Form II (in red) under LAG conditions.[10]

7 Quantitative analysis of the outcome of ball milling reactions

Ball-milling reactions are usually monitored in two ways:
1. **HPLC**, which requires dissolving the sample.
2. **PXRD**, which analyses the solid directly.

Each method has benefits and drawbacks.

7.1 Analysis by HPLC

HPLC is highly effective for the analysis of many organic reactions; however, its role in analytical chemistry is largely limited to the chemical analysis of such systems.[43] As an organic reaction proceeds, starting materials are converted into products with different chemical and physicochemical properties, often involving the incorporation of functional groups with varying polarities. These differences enable HPLC to effectively separate the compounds, referred to as analytes. In general, greater differences in these properties lead to improved separation of the analytes.

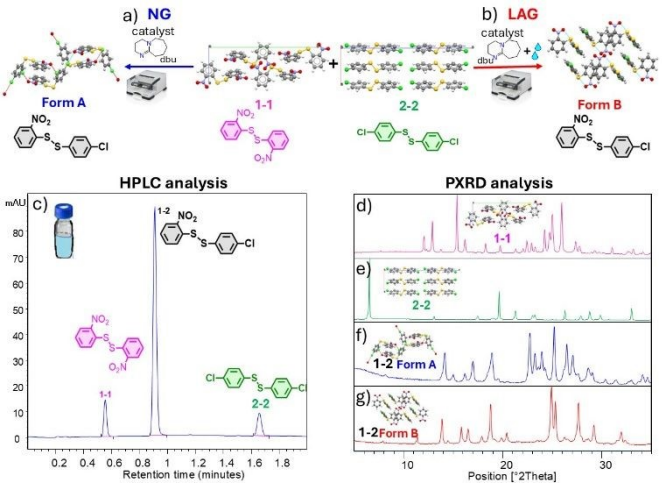

Figure 8 Synthetic scheme of ball mill disulfide exchange reaction under a) NG and b) LAG conditions Analysis of the products. c) by HPLC analysis and d) to g): by PXRD analysis showing PXRD patterns corresponding to crystal structures of (d) 1–1, (e) 2–2, and the polymorphs of the heterodimer 1–2 as (f) Form A and (g) Form B.[41, 44]

Figure 8c shows an example of HPLC analysis using a disulfide exchange reaction. To analyse a sample, the milled powder is fully dissolved in acetonitrile with a small amount of TFA to

View Article Online
DOI: 10.1039/D6CP00448B

neutralise the base (DBU) in the sample The samples is then injected into the HPLC. The size of each peak tells us how much of each compound is present (reported in mol%). A good HPLC method can clearly separate the two homodimers from the heterodimer product. The acidic solvent also prevents the disulfide exchange reaction from scrambling during preparation in solution.

HPLC is highly sensitive and can detect minor components down to approximately 0.1%. In disulfide exchange reactions, both homodimers (starting materials) are added in an accurate 1:1 stoichiometry; therefore, equimolar homodimers should produce peaks with equal areas in the HPLC chromatogram. The UV detection wavelength and bandwidth (260 nm, 8 nm bandwidth) were chosen empirically to ensure that both equimolar homodimers (1–1 and 2–2) give identical, or at least very similar, peak areas.[41]

In the disulfide exchange system, one equivalent of each homodimer forms two equivalents of the heterodimer. Under these conditions, the combined signals correspond to a total of 100 mol%. Accordingly, the composition of the powders is reported in mol%.

7.1.1 Limitations of HPLC

Bringing the sample of an organic reaction from the solid state into solution as required by HPLC, results in a significant loss of intrinsic sample information. This includes many of the unique physical processes associated with ball milling, such as polymorph formation, crystallite size, and studies on defect generation, and mechanical activation.

As an alternative to HPLC analyses, the same organic reaction could have been analysed both qualitatively and quantitatively in the solid state using PXRD. This approach provides access to the wealth of solid-state information, as discussed in Section 7.2.

HPLC is not suitable for the analysis of:

- cocrystals, as they dissociate into their constituent coformers upon dissolution. As a result, HPLC can only be used to verify that the coformers are present in the correct stoichiometric ratio.
- MOFs, as they are fully insoluble. However, the organic ligands that form the framework can be analysed by HPLC using elaborate sample preparation. This requires the use of strong chemicals to disassemble the ligands from the metal nodes, allowing the ligands to enter solution and become amenable to HPLC analysis.[45, 46]
- inorganic reactions, since the ions typically do not absorb UV light and are too polar for retention on reverse-phase HPLC columns. Solution-based techniques, such as Inductively Coupled Plasma (ICP) analysis are more practical for such systems.

In contrast, PXRD provides both chemical and phase composition and extensive solid-state structural information for cocrystals, MOFs and inorganic compounds.

7.2 Analysis by PXRD

Figures 8d–g show PXRD patterns for the disulfide system (discussed in Section 7.1), being analysed in the solid state. PXRD tells us what crystal forms are present.[47] The two disulfide homodimers give different patterns, and the heterodimer can appear as two different polymorphs. Using HPLC in combination with PXRD enables correlation of chemical transformations with concurrent changes in the solid state, as discussed further in Section 7.3.

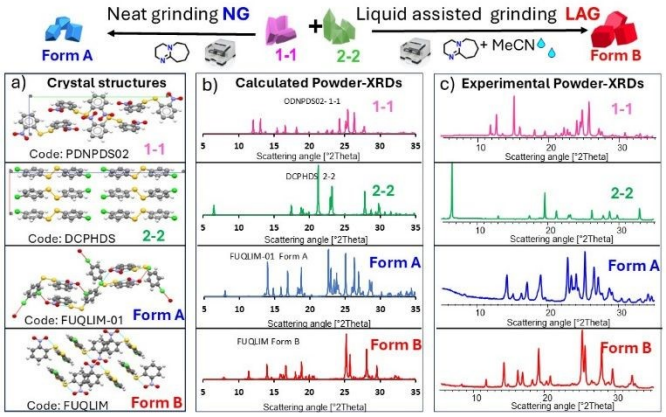

Figure 9 Disulfide exchange reaction of the homodimers 1-1 and 2-2 leading top left to the formation of Form A of 1-2 under NG conditions and top right to formation of Form B of 1-2 under LAG (MeCN) conditions. Column a) on the left, showing the crystal structure of 1-1, 2-2, Form A and Form B; b) in the middle, showing calculated PXRD patterns from the crystal structures listed in a); c) on the right, showing experimental PXRD scans obtained by running the pure samples of 1-1, 2-2, Form A and Form B of 1-2 in a diffractometer.[41, 44]

7.2.1 Strengths of PXRD

- PXRD preserves the sample in the solid state, providing insight into crystal structure, polymorphism, and crystallite size, while enabling investigation of mechanochemical processes such as microstrain, defect formation, and mechanical activation, particularly under in situ conditions. PXRD is suitable for organic reactions through the limit of detection (LOD) is poorer, ~3% instead of 0.1% by HPLC. PXRD is most suitable for cocrystals, supramolecular assemblies, MOFs, and inorganic systems—cases where HPLC fails.
- PXRD can also be quantitative when combined with the whole-pattern Rietveld refinement,[48] as long as the crystal structures of all components are known.[44] Figure 9a shows the crystalline structures, Figure 9b the calculated PXRD patterns,[44] and Figure 9c the experimental PXRD patterns for the compounds in the disulfide model system.
- PXRD can provide semi-quantitative information on crystallite size by applying the Scherrer equation within a whole-pattern Rietveld refinement, noting that the extracted values are subject to assumptions regarding peak broadening and microstrain.
- Ball-milling mechanisms can be studied using time-resolved in situ (TRIS) PXRD at synchrotron sources, enabling observation of intermediates inaccessible ex situ.

Examples include intermediate cocrystals,[49] and in situ polymorph transformations,[50] observed during Knoevenagel condensation reactions.

Ball milling usually produces very small crystals (a few to hundreds of nanometres).[10] Smaller nanocrystals give broader peaks in PXRD (Figure 10b), while larger ones give sharper peaks (Figure 10c).

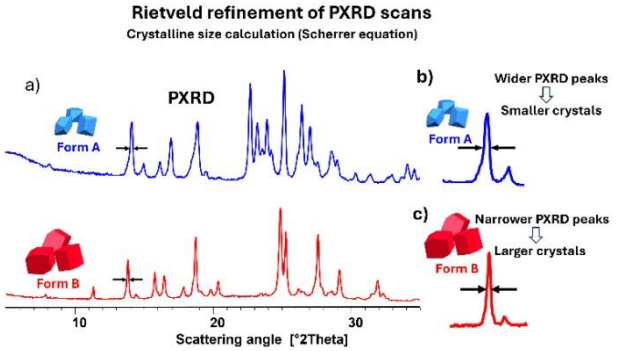

Figure 10 Evaluation of the Scherrer size. Schematic illustration of how nanocrystal size can be inferred from PXRD peak broadening. a) PXRD patterns of Form A of 1-2 (in blue) and Form B of 1-2 (in red); b) wider PXRD peaks indicate smaller crystals, c) narrower PXRD peaks indicate larger crystals.[10]

7.3 Comparing HPLC and PXRD quantitative results

Figure 11 shows that the kinetic curves prepared from HPLC and from the Rietveld refinement data calculated from PXRD patterns look almost the same. The reaction scheme of disulfide exchange under NG conditions is shown in Figure 11a.[51]

In Figure 11b, the kinetic profile shows the chemical makeup of the reaction mixture (in mol%) prepared from HPLC data. In Figure 11c, the kinetic profile shows the phase composition (also in mol%) prepared from Rietveld refinement data calculated from PXRD pattern.

Each data point in Figures 11b and 11c comes from a separate milling experiment. After each milling period, the powder was split and analysed in two ways:

HPLC to measure the molecular composition

PXRD to measure the solid phases present

The two kinetic profiles match very well. Using both methods together is powerful because each one confirms the results of the other. HPLC validates the PXRD data, and PXRD validates the HPLC data, which gives more confidence in the kinetics of the reaction.[51]

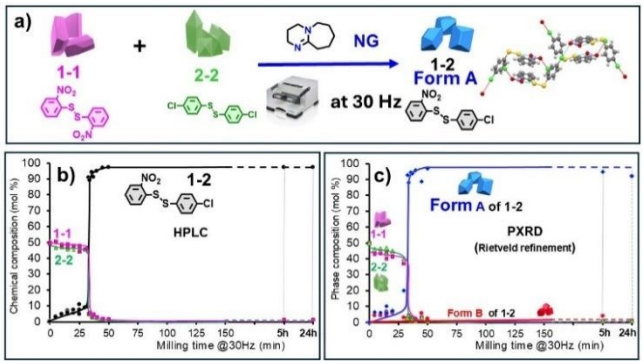

Figure 11. Kinetic profiles prepared by HPLC and PXRD data for the disulfide 1–2 reaction under NG conditions. (a) Reaction scheme. (b) Kinetic profile from molecular composition (HPLC). (c) Kinetic profile from phase composition (PXRD, Rietveld). Each point of the kinetic profile represents an independent milling experiment. The total 1–2 content in (b) reflects the combined Form A and Form B contributions determined in (c).[51] Adapted from Ref 51 with permission from JACS, 2014, 136, 16156-16166, Copyright {2014} American Chemical Society.

The PXRD results give an important extra detail. Figure 11c shows that only Form A of the heterodimer 1–2 appears during NG; Form B never forms at any time.

This means that the total amount of 1–2 measured by HPLC must equal the amount of Form A plus any Form B (if present), and only PXRD can tell us how much of each polymorph is there.

8 Is the outcome of solution-based and ball milling reactions always the same?

This is a particularly important question and is examined in detail throughout this section. The answer is NO, as clearly demonstrated by the data presented in Figures 12, 13 and 15. To address this issue, we use a simple disulfide exchange reaction as a model system. Two disulfide exchange reactions performed in solution (Section 8.1) are compared with their corresponding reactions carried out under ball-milling conditions (Sections 8.2.1–8.2.3). The scope of this comparison is further expanded by examining solution-based and ball-milling reactions involving three equimolar disulfide homodimers in the presence of DBU (Section 8.2.4).

8.1 Disulfide exchange reaction performed in solution

Disulfide exchange reactions in solution are reversible and operates under thermodynamic control.

In dilute solution, disulfide exchange reaction are well established within the field of dynamic covalent chemistry (DCC).[40] In solution (typically 1–5 mM), the exchange reaction between two equimolar homodimers reliably produces the corresponding heterodimer, and the system evolves toward a statistical equilibrium mixture. At equilibrium, the product distribution is consistently 25 : 25 : 50 mol% for homodimer a, homodimer b, and heterodimer ab, respectively.

This distribution arises because, in dilute solution, the thermodynamic stabilities of the two homodimers and the heterodimer are effectively identical. Under these conditions, the system follows purely statistical behaviour: since the heterodimer corresponds to two distinct molecular species (ab and ba) for every one molecule of each homodimer, the equilibrium composition naturally adopts the 25 : 25 : 50 ratio.

8.1.1 Disulfide 1-2 system performed in solution

We begin by considering the behaviour of the reaction in solution under standard DCC conditions. Figure 12a shows disulfide exchange reaction at 5 mM in MeCN in which the two

View Article Online
DOI: 10.1039/D6CP00448B

homodimers—1–1 (pink) and 2–2 (green)—scramble in the presence of the base catalyst DBU to form the heterodimer 1–2. The system evolves toward thermodynamic equilibrium (48h, stirring), where the heterodimer reaches 50 mol%. The HPLC trace shown at the bottom of Figure 12a confirms the expected statistical equilibrium composition of 25 : 50 : 25 mol% for 1–1 : 1–2 : 2–2, consistent with the well-established thermodynamic behaviour of disulfide exchange reactions in dilute solution.[41]

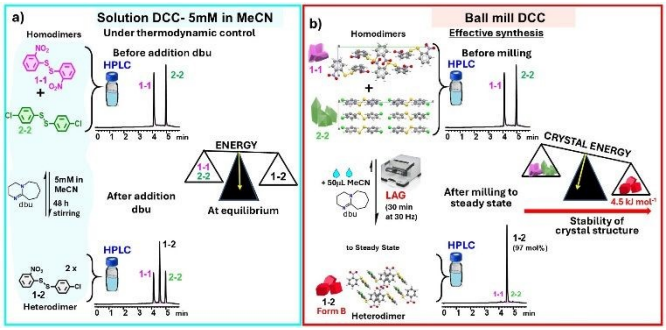

Figure 12 Comparison of solution-phase and ball-milling dynamic covalent chemistry (DCC) for the disulfide exchange between equimolar 1–1 and 2–2 in the presence of DBU, forming the heterodimer 1–2. (a) Solution DCC (5 mM in MeCN): top, before addition of DBU; bottom, after addition of DBU. (b) Ball milling DCC under LAG conditions (50 μL MeCN, 30 minutes at 30 Hz): starting from equimolar 1–1 and 2–2; top, before milling; bottom, after milling to steady-state. [41] Adapted from ref. 41 with permission from The Royal Society of Chemistry.

8.1.2 Disulfide 1-4 system

Figure 13a present a second solution based DCC example.
A 1 mM reaction in MeCN between two homodimers—bis(2-nitrophenyl) disulfide (1–1, pink) and bis(4-methylphenyl) disulfide (4–4, violet), scrambles in the presence of DBU to form the corresponding heterodimer 2-nitrophenyl-4-methylphenyl disulfide (1–4). The HPLC trace (Figure 13a) displays at the top the equimolar mixture of the starting materials 1-1 and 4-4, while after addition of DBU and stirring to equilibrium (48h) the HPLC trace displays at the bottom the expected statistical equilibrium composition of 25 : 50 : 25 mol% for 1–1 : 1–4 : 4–4, consistent with the thermodynamic behaviour of disulfide exchange in dilute solution.[41]

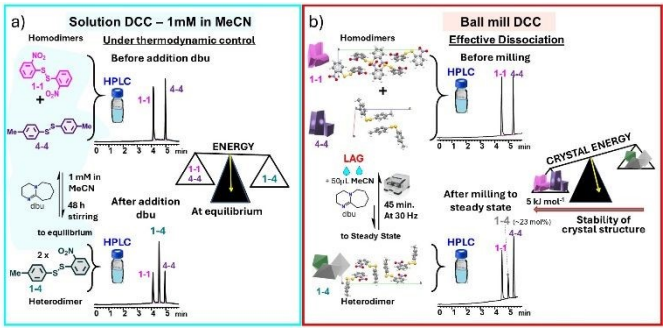

Figure 13 Comparison of solution-phase and ball-milling dynamic covalent chemistry (DCC) for the disulfide exchange between equimolar 1–1 and 4–4 in the presence of DBU, forming the heterodimer 1–4. (a) Solution DCC (1 mM in MeCN): top, before addition of DBU; bottom, after addition of DBU. (b) Ball milling DCC under LAG conditions (50 μL MeCN, 45 minutes at 30 Hz): starting from equimolar 1–1 and 4–4; top, before milling; bottom, after milling to steady-state.[41] Adapted from ref. 41 with permission from The Royal Society of Chemistry.

8.2 Disulfide exchange reactions under ball milling conditions

Under ball-milling conditions, disulfide exchange reactions eventually reach a steady-state, referred to in our previous publications,[10, 13, 39, 41, 51-53] as the "milling equilibrium"—at which the maximum product yield is obtained. Once this steady state is reached, further milling does not alter the composition, and both the physical and molecular states of the material remain constant for as long as the milling conditions are maintained.

8.2.1 Disulfide 1-2 system

For the reaction between 1–1 and 2–2 forming the heterodimer 1–2, a base catalyst (DBU) is required, as in solution-phase chemistry. Under LAG (50 μL acetonitrile) milled for 30 minutes at 30 Hz, 1–2 is obtained reproducibly in 97 mol% yield, with the remaining 3 mol% consisting of unreacted homodimers as presented in Figure 12b.[41] This contrasts sharply with solution-phase chemistry, where the heterodimer can only reach 50 mol% at thermodynamic equilibrium as in Figure 12a.
Notably, ball milling produces 1–2 as a single polymorph, Form B, under LAG conditions underscoring the influence of crystal structure in the solid state. The driving force for this high yield "effective synthesis" arises from the overall relative stability of the product crystal compared with the reactants.
Using the reported crystal structures of the homodimers and heterodimer, the average intermolecular interaction energy in the homodimer crystals is more stabilising than in the heterodimer crystal. However, the homodimers are overall disfavoured, as the 2–2 homodimer adopts a relatively high-energy conformation in its crystal structure. As a result, Form B of 1-2 is calculated to be 4.5 kJ mol^{-1} more stable than the corresponding homodimer starting materials.[41]
Similarly, NG of the same reactants leads to the formation of Form A, which is likewise more stable than the homodimers by the same energy difference.[41]
This principle of effective synthesis, where the overall relative stabilities of the crystalline products dictate the reaction outcome, has been observed consistently across other disulfide exchange reactions under both LAG and NG conditions.

8.2.2 Disulfide 1-3 system

The ball-milling disulfide exchange 1–3 system provides a particularly compelling illustration of how mechanochemical conditions dictate steady-state composition. Milling the homodimers bis(2-nitrophenyl) disulfide (1–1) and bis(4-nitrophenyl) disulfide (3–3) in the presence of DBU leads to markedly different outcomes depending on whether the reaction is performed under NG or LAG with MeCN.
Under LAG conditions, the reaction proceeds to near-quantitative formation of the heterodimer (2-nitrophenyl-(4-nitrophenyl) disulfide 1–3, which is obtained exclusively as Form B, reaching >99 mol% (Figure 14a).[53]

View Article Online
DOI: 10.1039/D5CP00448B

In sharp contrast, NG conditions lead to a distinct steady-state in which Form A of 1–3 is obtained as the major product (80–85 mol%), while the remaining 15–20 mol% consists of an equimolar mixture of the homodimers 1–1 and 3–3 (Figure 14b).[53]

Although the crystal stability of the 1–3 disulfide system has not been explicitly calculated, the outcomes from NG and LAG can infer that the key factors governing stability—and thus the driving forces of the ball milling reaction, may be consistent with those identified for the 1–2[41] and 1–4[41] systems (Sections 8.2.1–8.2.3). For the 1–1 + 3–3 system, the total crystal structure energy (defined as the sum of intermolecular interactions and the molecular conformational energy within the crystals) favours heterodimer formation, more strongly for Form B (>99.5 mol%) than for Form A (~80–85 mol%).

Figure 14 Effect of milling conditions on the 1-1 + 3-3 disulfide exchange in the presence of DBU. Under NG conditions (left), the reaction yields mostly Form A of 1-3 (80–85 mol%), with 15–20 mol% unreacted 1-1 and 3-3. Under LAG conditions (right), Form B of 1-3 is obtained quantitatively.[41, 53]

8.2.3 Disulfide 1-4 system

Not all mechanochemical reactions lead to quantitative product formation at steady-state. In some cases, the driving force favours the starting materials rather than the product, as illustrated in Figure 13b.

For example, ball milling an equimolar mixture of 1–1 and 4–4 under LAG conditions (50 μL acetonitrile, 45 minutes and longer, 30 Hz) in the presence of DBU yields only 23–24 mol% of the heterodimer 1–4 at steady-state.

The total crystal energies, evaluated as the sum of intermolecular interactions and the intramolecular conformational energy within the crystal structures, favour the homodimers over the heterodimer by 4.5 kJ mol^{-1}. Accordingly, the homodimer crystal structures (1–1 and 4–4) are calculated to be 4.5 kJ mol^{-1} more stable than the heterodimer (1–4) under LAG conditions. We refer to this phenomenon as an "effective dissociation".[41]

8.2.4 Disulfide: 1-2 & 1-3 & 2-3 systems:

To explore this system further, we examined the disulfide exchange of an equimolar mixture of three homodimers (1–1, 2–2, and 3–3) under base-catalysed ball-milling conditions. This reaction generates the three corresponding heterodimers (1–2, 1–3, and 2–3; Figure 15a and c).[41]

In solution, the reaction reaches thermodynamic equilibrium, producing a statistical mixture of the three homodimers and three heterodimers, as confirmed by HPLC analysis (Figure 15b).

Under ball mill LAG (Figure 15d), the steady-state product distribution differs markedly from that in solution. The relative composition of homodimers and heterodimers are governed by the overall relative stabilities of their crystalline phases. Heterodimer 1–3 appears most stable, exhibiting the largest HPLC peak, followed closely by 1–2, which leads to complete consumption of 1–1 homodimer. In contrast, heterodimer 2–3 is the least stable, leaving residual 2–2 and 3–3 homodimers in the mixture at steady-state.[41]

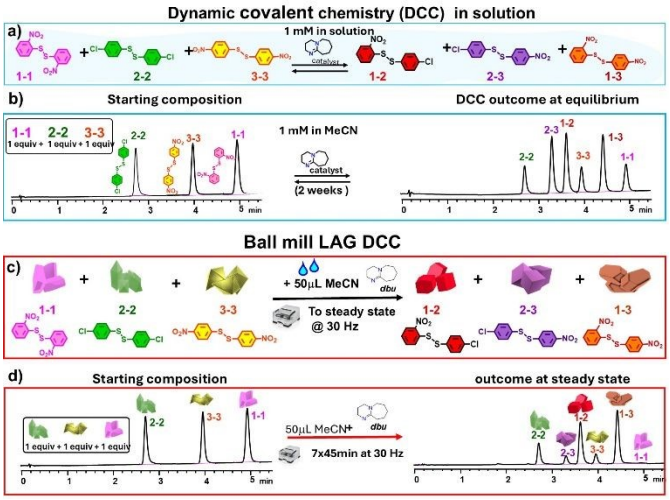

Figure 15 Outcome of disulfide exchange among three equimolar homodimers (1–1, 2–2, 3–3) in the presence of DBU leading to the formation of 3 heterodimers 1-2, 2-3,1-3. a) & b) solution DCC (1 mM, MeCN) of three equimolar homodimers (1–1, 2–2, 3–3) in the presence of DBU; a) Reaction scheme; (b) outcome of solution DCC at steady-state monitored by HPLC. c&d) ball mill LAG (MeCN) of three equimolar homodimers (1–1, 2–2, 3–3) in the presence of DBU. c) reaction scheme; d) outcome of ball mill LAG milled to steady-state and monitored by HPLC.[41] Adapted from ref. 41 with permission from The Royal Society of Chemistry.

8.3 Lessons learned

Under thermodynamic equilibrium in solution, the heterodimer can reach a maximum of only 50 mol%, with the remaining 50 mol% comprising an equimolar mixture of the two homodimers (Figures 12a and 13a). This scrambling behaviour is characteristic of the disulfide exchange reactions of homodimers in solution that we have investigated, both in our published work[41, 53, 54] and in additional unpublished studies. Indeed, disulfide exchange reactions conducted in solution invariably converge to a statistical distribution of homo- and heterodimers at equilibrium.[41]

9 Dynamic nature of ball milling

Just as disulfide bonds continuously break and reform under base-catalysed conditions in solution-based DCC reactions, the same behaviour is observed under ball-milling conditions in the presence of a base catalyst (DBU). In the absence of DBU, no bond cleavage or reformation occurs.

Consistent with disulfide exchange solution-based DCC, the steady-state outcome of ball-milling reactions of disulfide homodimers in the presence of DBU can be achieved from any

View Article Online
DOI: 10.1039/D5CP00448B

initial composition, provided the starting materials are supplied in the correct stoichiometric ratios.

9.1 Disulfide 1-4 system

To illustrate the intrinsically dynamic nature of ball-milling reactions, we consider the LAG "effective dissociation" of an equimolar mixture of 1–1 and 4–4 milled to steady-state in the presence of DBU. Irrespective of the initial form of the starting material, the system reproducibly converges to the same steady-state composition (4:2:4 for 1–1:1–4:4–4). This composition is obtained whether milling is initiated from an equimolar mixture of 1–1 and 4–4 (Figures 13b and 16b) or from the pure heterodimer 1–4 (Figure 16c).[41]

The defining requirement is that the starting material contains, or is derived from, the correct overall stoichiometric ratio of the disulfide building blocks. Accordingly, the identical steady-state (4:2:4 for 1–1:1–4:4–4) would also be reached starting from a statistical mixture (1:2:1 for 1–1:1–4:4–4) or from any intermediate composition sampled during the milling process. This behaviour demonstrates that mechanochemical reactions explore a dynamic compositional landscape and converge to a stoichiometry-defined steady-state rather than retaining a memory of the initial molecular distribution.[41]

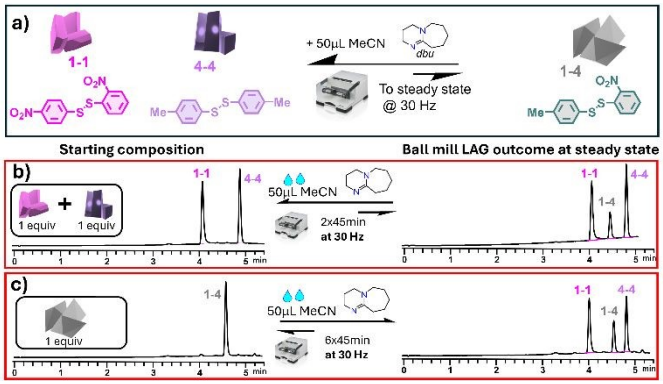

Figure 16 Steady-state composition is independent of the initial state of the starting material when stoichiometry is conserved. (a) Scheme of the equimolar LAG reaction between 1-1 and 4-4. (b–c) Milling in the presence of DBU gives the same steady-state composition (4:2:4 for 1-1:1-4:4-4) whether starting from b) an equimolar 1-1/4-4 mixture or c) from pure 1-4.[41] Adapted from ref. 41 with permission from The Royal Society of Chemistry.

9.2 Disulfide: 1-2 + 1-3 + 2-3 system

The dynamic nature of disulfide exchange under ball-milling conditions in the presence of DBU can be further demonstrated by deliberately perturbing the steady-state composition through the introduction of an additional homodimer. Using the same disulfide system shown in Figure 15c, milling equimolar quantities of 1–1, 2–2, and 3–3 under LAG conditions produces the steady-state composition depicted in Figures 15d and 17b.

Strikingly, the identical steady-state is reached when the reaction is initiated from alternative starting mixtures that differ substantially in molecular composition. For example, beginning with two equivalents of 1–2, obtained quantitatively from the LAG reaction of 1–1 and 2–2 (Figure 12b), and subsequently adding one equivalent of 3–3 leads to the same final composition (Figure 17c). Likewise, starting from two equivalents of 1–3, generated by LAG with MeCN from 1–1 and 3–3 (Figure 14a), followed by the addition of one equivalent of 2–2, again converges to the same steady-state (Figure 17d).[41]

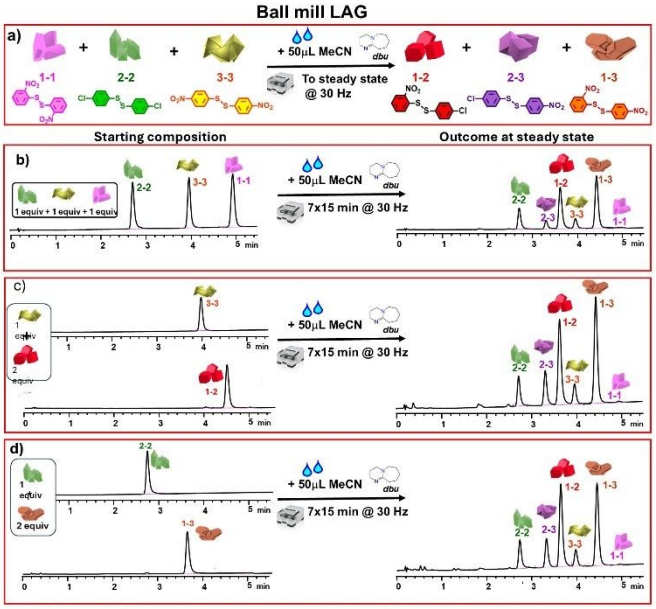

Figure 17 Steady-state composition under ball milling is independent of the starting point when overall stoichiometry is conserved. (a) Scheme of the equimolar LAG reaction of 1-1, 2-2, and 3-3 with DBU to steady-state, forming heterodimers 1-2, 1-3, and 2-3. (b–d) The same steady-state molecular distribution is reached whether starting from: (b) 1 equivalent each of 1-1, 2-2, and 3-3; (c) 2 equivalents of 1-2 plus 1 equivalent of 3-3; or (d) 2 equivalents of 1-3 plus 1 equivalent of 2-2.[41] Adapted from ref. 41 with permission from The Royal Society of Chemistry.

9.3 Lessons learned

These experiments provide direct evidence that mechanochemical steady-states are stoichiometry-controlled and dynamically maintained, rather than being determined by the initial molecular distribution.[41]

10 Determinants of steady-state outcomes in ball milling reactions.

Here, we aim to demonstrate that the outcome of ball-milling reactions does not depend on external factors such as the physical state of the base catalyst (semi-liquid versus solid), but rather on the milling conditions themselves. This is illustrated by examining whether replacing DBU with a solid base catalyst affects the steady-state composition in two model disulfide systems; 1–2 (Section 10.1) and 1–3 (Section 10.2) under both NG and LAG conditions.

10.1 Disulfide exchange ball milling using base catalysts in solid form

View Article Online DOI: 10.1039/D5CP04498B

These experiments were motivated by the concern that the outcomes observed with DBU—a viscous liquid catalyst—might not be generalisable to solid-state catalysts.

All ball mill reactions presented in this chapter were performed in a home-made 14.5 mL stainless steel milling jar with two 7 mm diameter stainless steel balls. The loaded milling jar with 200 mg of powder was installed on a Retsch MM400 ball mill and milled at 30 Hz.

10.2 Disulfide 1-2 system

To address this concern, we examined the 1–2 disulfide exchange system using nine commercially available solid amine catalysts under both NG and LAG conditions. The results, summarised in Figure 18, show that all solid catalysts produced the same steady-state outcome as with DBU as monitored by HPLC. Under NG conditions, Form A of 1-2 is obtained at ~97 mol%. Under LAG conditions with 50 µL MeCN, Form B of 1-2 is obtained at ~97 mol%. The mayor differences between the use of different catalysts were in the reaction rates. Under NG conditions, DBU reached steady-state in 45 min, whereas the solid catalysts required between 3 and 24 h. Under LAG conditions DBU and most other solid-based catalysts reached steady-state with a few exception, which required 3h milling.[54]

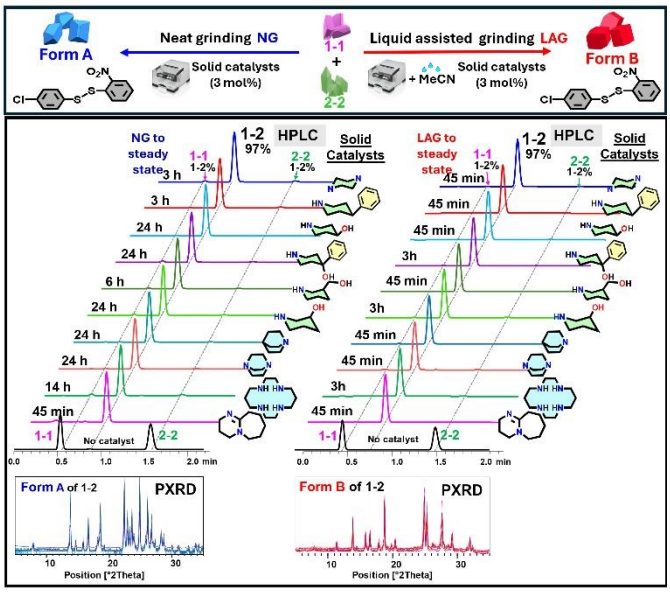

Figure 18 Steady-state formation of 1-2 under NG and LAG conditions using 9 commercially available solid base catalysts and DBU. Top: Reaction scheme showing that NG produces Form A of 1-2, while LAG with MeCN yields Form B of 1-2. Left: NG reactions (3 mol% catalyst) milled to steady-state yields Form A to ~97 mol% with matching PXRD patterns below; right: LAG (MeCN) reactions with (3 mol% catalyst) milled to steady-state yields Form B to ~97 mol%. Despite consistent steady-state outcomes (Form A and Form B), the reaction kinetics vary significantly across base catalysts used specially under NG conditions.[54] Adapted with permission from Ref 54 [ChemSusChem, 2022, 15, e202102416]. Copyright [2022] Wiley-VCH GmbH.

10.3 Disulfide 1-3 system

In a parallel set of experiments, we investigated the 1–3 disulfide system using the same nine solid amine catalysts. Remarkably, the outcome was identical to that observed with DBU. Under NG conditions, Form A of 1–3 was consistently obtained at ~85 mol% at steady-state, whereas under LAG conditions with MeCN, Form B formed in >99 mol% yield (Figure 19), reproducing the behaviour shown previously in Figure 14. The only variation among the catalysts was in reaction kinetics, which differed significantly depending on the specific solid amine used.[54]

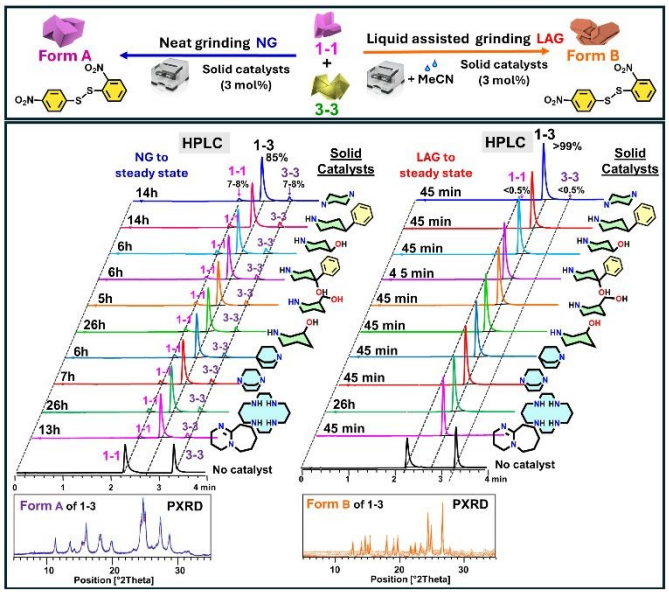

Figure 19 Steady-state formation of 1-3 under NG and LAG conditions using solid base catalysts. Top: Reaction scheme showing that NG produces Form A of 1-3, while LAG with MeCN yields Form B of 1-3. Left: NG reactions (3 mol% catalyst) give ~85 mol% Form A of 1-3, with the remaining 1-1 and 3-3 present at ~7–8 mol% each; with matching PXRD patterns below. Right: LAG reactions give >99 mol% Form B of 1-3, with matching PXRD patterns below. Despite consistent steady-state outcomes (Form A vs. Form B), the reaction kinetics vary significantly across base catalysts used specially under NG conditions.[54] Adapted with permission from Ref 54 [ChemSusChem, 2022, 15, e202102416]. Copyright [2022] Wiley-VCH GmbH.

10.4 Lessons learned

For all disulfide exchange reactions investigated under NG and LAG conditions, the steady-state outcome is independent of whether a liquid or solid catalyst is used; only the reaction kinetics vary with the choice of catalyst.

11 Kinetic profiles of NG and LAG reactions without and with added seeds of heterodimer

All ball mill reactions presented in this section were performed in a home-made 14.5 mL stainless steel milling jar with two 7 mm diameter stainless steel balls. The loaded milling jar with 200 mg of powder was installed on a Retsch MM400 ball mill and milled at 30 Hz.

11.1 Unseeded kinetic profiles of 1-2 disulfide system

When the disulfide homodimers 1–1 and 2–2 are milled in the presence of any base catalyst, the reaction to 1-2 disulfide heterodimer always reaches the same steady-state outcome:

- **NG:** only Form A of 1–2 is exclusively and quantitatively formed (Figure 20b).
- **LAG:** only Form B of 1–2 is exclusively and quantitatively formed (Figure 20c).

What happens before steady-state, however, is less obvious. To clarify this, we monitored the reaction kinetic profile. Because the fundamental principles of ball milling are still being developed, classical solution-state terms such as “stable” and “unstable” (valid under ambient pressure and temperature in solution chemistry) are not appropriate. Instead, we adopt terminology reflecting observations under ball milling conditions:

Persistent polymorph: the polymorph that persists under a given set of milling conditions.

Short-lived polymorph: the polymorph that, if present, cannot survive long under the given milling conditions and is eventually consumed.

When the reaction is followed over time, both NG and LAG exhibit three kinetic stages:[30]

1. **Induction stage** – initially, no apparent reaction occurs. During this stage, the crystals of the starting materials are mechanically weakened: particles fracture, defects accumulate, and the solid becomes more reactive. This gradual destabilization primes the system for reaction.
2. **Reaction stage** – once sufficient defects have accumulated, the reaction proceeds rapidly, yielding a sigmoidal (S-shaped) kinetic curve as reactants are consumed and product forms.
3. **Steady-state** – the composition reaches a plateau where no further changes occur. At this stage, the product has attained its maximum achievable yield under the chosen milling conditions, and both molecular and phase compositions remain constant. Remarkably, this steady-state composition does not change even after prolonged milling (e.g., 5 h or 24 h), whether under NG or LAG conditions (Figure 20).

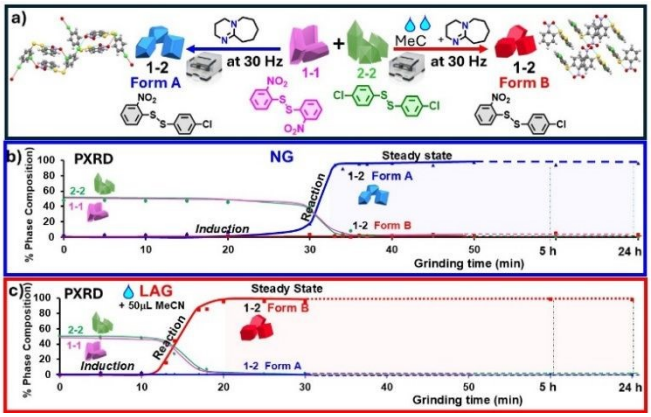

Figure 20 Kinetics profile of 1-2 disulfide formation under NG and LAG conditions with DBU. (a) Mechanochemical scheme: equimolar 1-1 + 2-2 with DBU yields Form A of 1-2 under NG (left) and Form B of 1-2 under LAG (right); (b) NG kinetic profile (c) LAG kinetic profile. Kinetic profiles prepared from Rietveld refinement data of PXRD patterns. Each point of the kinetic profile represents an independent experiment.[51]

Adapted from Ref 51 with permission from JACS, 2014, 136, 16156-16166, Copyright {2014} American Chemical Society.

Why the system remains unchanged despite continued mechanical agitation is an active topic of theoretical debate. In systems with reversible covalent bonds, such as disulfides, bonds continue to break and reform in the presence of a base catalyst, yet the overall composition remains fixed once steady-state is reached.[51]

Experimentally, crystallite size also remains essentially constant at steady-state, even under extended milling (See Section 13.1). Understanding the mechanisms that maintain this steady-state crystallite size is emerging as a distinct research area, with potential to reveal new fundamental principles of ball milling.[55]

11.2 Kinetic profile of 1-3 system

In the ball-mill reaction of the 1–2 disulfide system in the presence of DBU, both NG (Figure 20b) and LAG (Figure 20c) conditions lead to quantitative product formation of ~97 mol%. This behaviour was found not to be universal, as demonstrated by the 1–3 disulfide system.[53]

For the 1–3 system, NG conditions afford Form A of 1-3 at only 80–85 mol% at steady-state, with 1–1 and 3–3 persisting at 8–10 mol% (Figure 21b). This composition remains unchanged even after 24 h of continuous milling.[53]

In contrast, under LAG conditions (Figure 21c), Form B of 1-3 is formed quantitatively (>99 mol%), fully consuming the homodimers 1-1 and 3-3. The LAG reaction also reaches steady-state much more rapidly (~15 minutes) compared with the NG reaction, which requires nearly 2 h.[53]

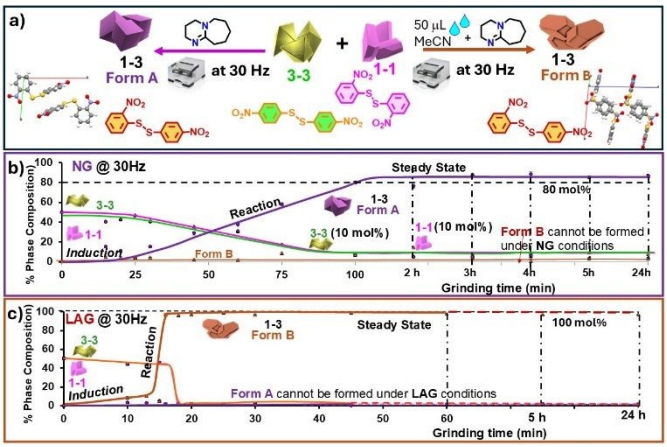

Figure 21 Ball-milling reactions of 1-1 and 3-3 under NG and LAG conditions with DBU. (a) Mechanochemical scheme: left-NG yields Form A of 1-3 while right-LAG yields Form B of 1-3. (b, c) Kinetic profiles prepared from Rietveld refinement data of PXRD scans, b) under NG, Form A of 1-3 forms exclusively at 80–85 mol%, with 15–20 mol% residual 1-1/3-3; c) Under LAG with 50 µL MeCN Form B of 1-3 forms exclusively at >99 mol%. Each point of the kinetic profile represents an independent experiment.[53] Adapted with permission from Ref [53]. Copyright [2021] Wiley.

11.3 Seeded kinetic profiles of 1-2 disulfide system in the presence of DBU

View Article Online
DOI: 10.1039/D6CP00448B

Seeding experiments of either polymorph of the reaction product in the disulfide model system it allows to examine how introducing crystalline seeds into an equimolar mixture of disulfide homodimers affects the kinetics of ball milling reactions.

This chapter presents experimental evidence for two contrasting cases, of adding seeds or the persistent or the short lived polymorphs to equimolar mixture of homodimers.

These studies reveal how seeding influences nucleation behaviour, reaction rates, but not the steady-state composition of mechanochemical disulfide exchange reactions.

11.3.1 Addition of seeds of persistent polymorph of 1-2 disulfide in presence of DBU

Figures 22 and 23 confirm the expected behaviour: adding small amounts (as little as 3 mol%) of seeds of the persistent polymorph of 1-2 to 97%mol of an equimolar mixture of the homodimers 1-1 and 2-2 in the presence of DBU, accelerates the reaction on milling at 30 Hz as monitored by PXRD.[51]

Under LAG conditions, the seeds of the persistent polymorph of 1-2 which are added as 3 mol% is Form B (Figure 22), whereas under NG conditions it is Form A (Figure 23). As anticipated, this seeding effect is clearly visible.[51]

Under NG conditions, seeding with the persistent polymorph of 1–2 significantly shortens the induction stage (Figure 23b). Under LAG conditions, the induction stage appears to be eliminated relative to the unseeded reaction (Figure 22b). However, it should be noted that the earliest ex situ milling time point that can be analysed corresponds to 1 minute after the start of milling. Consequently, any induction period occurring between 0 and 1 minute cannot be excluded. In both under NG and LAG conditions, only minor differences are observed in the steepness of the sigmoidal growth stage when comparing seeded and unseeded reaction kinetics.[51]

Importantly, the steady-state phase composition remains unchanged when reactions are seeded with respect to unseeded reactions; with the persistent polymorph under NG (Figure 23b) or LAG (Figure 22b) conditions. Seeded reactions under LAG conditions reach steady-state much earlier than under NG conditions.[51]

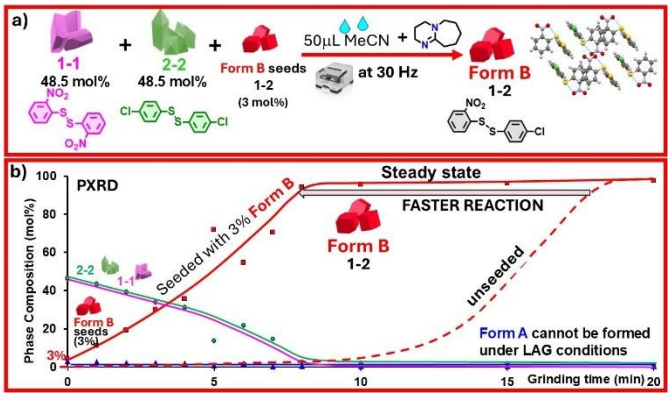

Figure 22 Effect of Form B of 1-2 (persistent polymorphs under LAG) seeded at 3 mol% on the LAG reaction of 1-1 and 2-2 with DBU. (a) Reaction scheme: (b) Kinetic profile between seeded and unseeded experiments prepared from Rietveld refinement data of PXRD patterns. Each point of the kinetic profile represents an independent experiment.[51] Adapted from Ref 51 with permission from JACS, 2014, 136, 16156-16166, Copyright {2014} American Chemical Society.

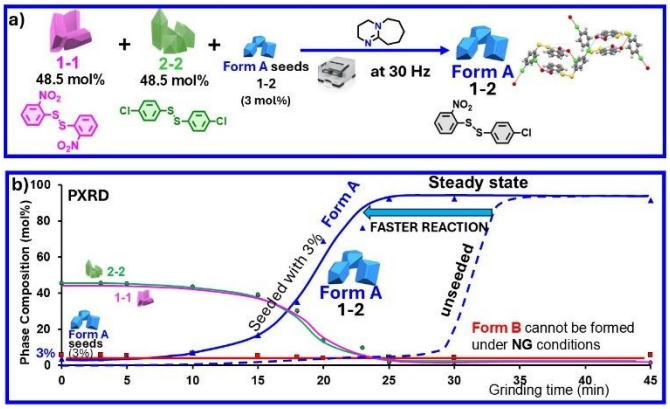

Figure 23 Effect of Form A of 1-2 (persistent polymorph under NG) seeded at 3 mol% on the NG reaction of 1-1 and 2-2 with DBU. (a) Reaction scheme: (b) Kinetic profile between seeded and unseeded experiments prepared from Rietveld refinement data of PXRD patterns. Each point of the kinetic profiles represents an independent experiment.[51] Adapted from Ref 51 with permission from JACS, 2014, 136, 16156-16166, Copyright {2014} American Chemical Society.

11.3.2 Addition of short-lived polymorph seeds of 1-2 disulfide in presence of DBU

To assess the behaviour of short-lived polymorphs under milling, 3 mol % seeds of Form A of 1-2 (under LAG conditions) or Form B of 1-2 (under NG conditions) were added to 97 mol% of an equimolar mixture of the homodimers 1-1 and 2-2 in the presence of DBU. Because PXRD cannot reliably detect phases present below ~3 mol%, initial experiments were monitored by HPLC.[51] These results were subsequently confirmed using 23 mol% of seeds of short-lived polymorphs of 1-2 added to 77 mol% of an equimolar mixture of the homodimers 1–1 and 2–2 in the presence of DBU. At this loading of 23 mol%, the short-lived polymorphs are readily detectable by PXRD, allowing the progress of the kinetic studies to be monitored directly.[51]

11.3.2.1 Addition of short-lived polymorph seeds of 1-2 disulfide under LAG conditions in the presence of DBU.

Adding 23 mol% of Form A seeds of 1-2 (short-lived polymorph) to 77 mol% of an equimolar 1–1/2–2 mixture and milled at 30 Hz under LAG conditions (50µL MeCN) in the presence of DBU, led to very rapid disappearance of the seed as monitored by PXRD (Figure 24b). This behaviour mirrored that previously observed seeding only with 3 mol% of Form A (figure not included). Form A of 1-2 fell from 23 to ~5 mol% within the first minute of milling as per HPLC analysis (see insert Figure 24b). This was accompanied by a simultaneous increase in the levels of each of the homodimers 1-1 and 2-2 from 38.5 mol% to just below 50 mol% (Figure 24b). Beyond this initial 1 minute stage (framed in blue), the reaction proceeded identically to unseeded controls (Figure 20b) and later converged to the same

View Article Online
DOI: 10.1039/D5CP04148B

steady-state composition resulting the formation of Form B of 1-2 at 97 mol%.

Seeded reactions with the short-lived polymorph showed a slight acceleration with respect to unseeded, attributable to two parallel pathways as explained in Figure24c: (i) a dominant sequential pathway in which the seeds of Form A undergo disulfide exchange to regenerate the homodimers 1-1 and 2-2. These then react by disulfide exchange in the presence of DBU to form the persistent polymorph Form B of 1-2 after milling for 10 minutes, and (ii) a minor direct solid–solid interconversion from Form A to Form B of 1-2. Early formation of Form B of 1-2 through the minor direct pathway may account for the modest rate enhancement, without affecting the final steady-state composition.[51]

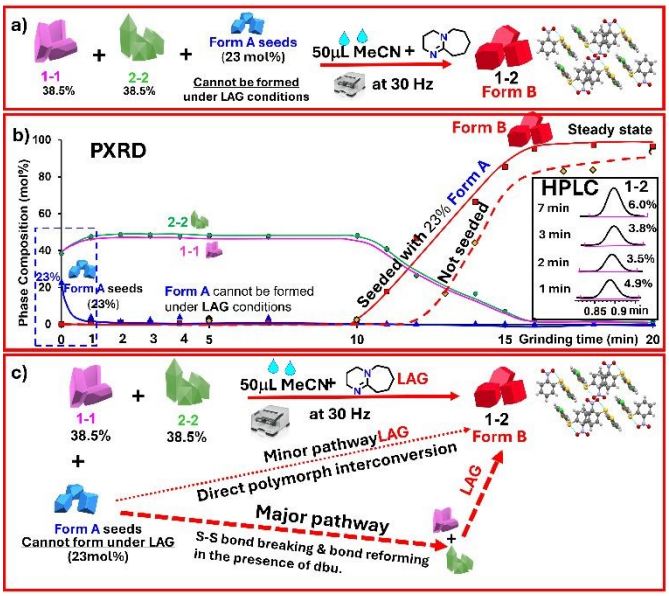

Figure 24 Effect of addition of 23 mol% short-lived Form A seeds of 1-2 on the LAG reaction of 1-1 and 2-2 with DBU. (a) Reaction scheme (b) Kinetic profile prepared from Rietveld refinements of PXRD scans, and from HPLC data (inset). (c) Mechanistic insight. Each point in the kinetic profile represents an independent experiment.[51] Adapted from Ref 51 with permission from JACS, 2014, 136, 16156-16166, Copyright {2014} American Chemical Society.

11.3.2.2 NG condition: addition of short-lived polymorph seeds of 1-2 disulfide in the presence of DBU

When 23 mol% of Form B (short-lived polymorph) was added to 77 mol% of an equimolar 1–1/2–2 mixture and milled at 30 Hz under NG conditions in the presence of DBU (Figure 25b), its behaviour mirrored that previously seen with 3 mol% seeds of Form B (figure not included). The kinetic profile prepared with the Rietveld refinement of the PXRD scans is presented in Figure 25b and the relevant HPLC data is presented in the insert. It shows that the 23 mol% seeds of Form B of 1-2 predominantly undergoes direct interconversion to Form A of 1-2, the persistent polymorph under NG conditions.[51]

This proposed hypothesis is illustrated in Figure 25c. A sequential pathway via homodimers appears minor; this is supported by the composition of 1–1 and 2–2 remaining essentially unchanged during the first 15 minutes of milling as monitored by PXRD and HPLC. Consistent with this, the signal for Form B as monitored by PXRD does not decrease on milling. Monitoring the fate of 1-2 (Form A + Form B) by HPLC shows that it slightly increases (from initial 23 mol% to 24.4 mol% at 5 min. and 27.7 mol% at 10 min as presented in insert in Figure 25b). The resulting sigmoidal kinetic profile reflects direct conversion of Form B to persistent Form A of 1-2 which outpaces the slower pathway involving homodimer formation as depicted in Figure 25c.[51]

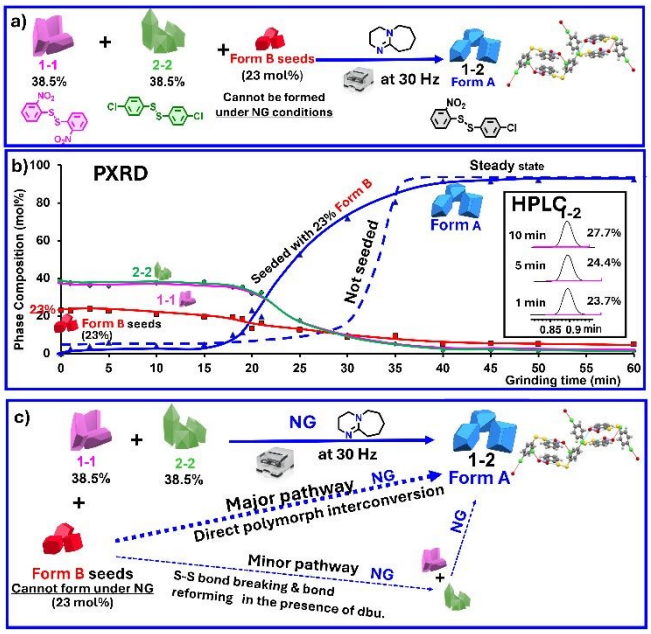

Figure 25 Effect of addition of 23 mol% short-lived Form B seeds of 1-2 on the NG reaction of 1-1 and 2-2 with DBU. (a) Reaction scheme (b) Kinetic profile prepared from Rietveld refinements of PXRD scans, and from HPLC data (inset). (c) Mechanistic insight. Each point in the kinetic profile represents an independent experiment.[51] Adapted from Ref 51 with permission from JACS, 2014, 136, 16156-16166, Copyright {2014} American Chemical Society.

11.4 Addition of seeds of short-lived polymorph of 1-2 in the absence of DBU

All disulfide heterodimers must be prepared via disulfide exchange from the corresponding homodimers in the presence of DBU. The disulfide heterodimers Form B of 1–2 can be recrystallised from methanol, isopropanol, or acetonitrile. Care must be taken to add trifluoroacetic acid (TFA) to the recrystallization solution to neutralize DBU; otherwise, even trace amounts of residual base catalyse disulfide exchange, leading to scrambling of the heterodimer in solution and convergence to the statistical limit of 50 mol% heterodimer.

To ensure that the isolated heterodimer is free of DBU, the crystals must be thoroughly washed to remove residual DBU and TFA.

As shown in Section 11.3.2.2. direct polymorph interconversion pathway does not require disulfide bond breaking and reforming, suggesting that short-lived seeds may transform even in the absence of DBU.[51]

11.4.1 LAG in absence of DBU: addition of short-lived seeds to 1-2 disulfide system

View Article Online
DOI: 10.1039/D6CP00448B

As Form A (the bulk metastable form) could not be recrystallised to yield crystals of Form A and so remove DBU, these experiments were instead performed by adding enough TFA to Form A powder containing 3 mol% DBU from the synthesis, thereby quantitatively quenching DBU in situ.

To test this, 23 mol% of short-lived Form A of 1-2 with neutralised DBU was added to an equimolar 1-1/2-2 mixture and milled at 30 Hz under LAG conditions (50μL MeCN) (Figure 26). As expected, no disulfide exchange occurred, and the concentrations of 1-1 and 2-2 remained constant. Nevertheless, Form A of 1-2 was quantitatively converted into the persistent polymorph (Form B), demonstrating that the greater stability of Form B under LAG conditions (see section 12.2) is sufficient to drive polymorph interconversion under ball milling conditions. This confirms that the direct pathway operates independently of covalent bond exchange and highlights the central role of lattice dynamics in governing polymorphic outcomes during milling.[51]

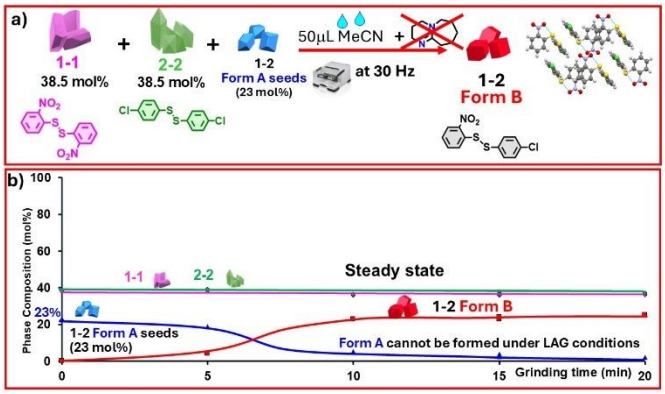

Figure 26 LAG reaction of 1-1 and 2-2 with seeds of 23 mol% short-lived crystals of Form A in the absence of DBU. (a) Reaction scheme (b) Kinetic profile prepared from Rietveld refinements data of PXRD scans. Each point in the kinetic profile represents an independent experiment.[51] Adapted from Ref 51 with permission from JACS, 2014, 136, 16156-16166, Copyright {2014} American Chemical Society.

11.4.2 NG in absence of DBU: addition of short-lived seeds to 1-2 disulfide system

In a similar way, 23 mol% seeds of crystals of Form B of 1-2 (short-lived polymorph) when added to 77 mol% of an equimolar 1–1/2–2 mixture and milled in the absence of DBU at 30 Hz under NG conditions, were fully transformed into the persistent polymorph (Form A), via direct polymorph interconversion (Figure 27). As expected, no disulfide exchange occurred in the absence of DBU, and the concentrations of 1-1 and 2-2 remained constant during milling.[51]

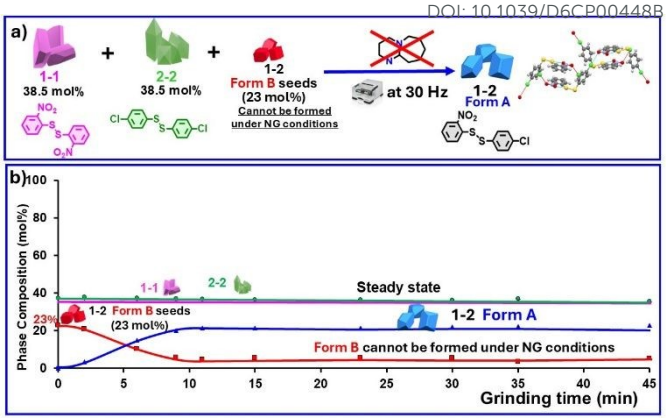

Figure 27 NG reaction of 1-1 and 2-2 with 23 mol% short-lived Form B seeds in the absence of DBU. (a) Reaction scheme (b) Kinetic profile prepared from Rietveld refinements of PXRD scans. Each point in the kinetic profile represents an independent experiment.[51] Adapted from Ref 51 with permission from JACS, 2014, 136, 16156-16166, Copyright {2014} American Chemical Society.

11.5 Lessons learned

Ball-milling reactions proceed through three distinct stages: induction, reaction, and steady state, at which point the maximum yield is achieved. LAG exhibits faster kinetics than NG. Reactions become reproducible upon reaching the steady state, as further milling does not alter the phase composition once the maximum yield has been attained.

The milling conditions (LAG or NG) dictate which polymorph of the product is exclusively formed, referred to as the persistent polymorph, throughout the kinetic study. The alternative polymorph is not detected at any stage and is therefore considered a short-lived polymorph. Under LAG conditions, Form B is the persistent polymorph, while Form A is short-lived. Conversely, under NG conditions, Form A is the persistent polymorph and Form B is short-lived.

The addition of seeds of the persistent polymorph of the disulfide heterodimer to an equimolar mixture of homodimers in the presence of DBU significantly accelerates the reaction, with a more pronounced effect under LAG than NG conditions.

In contrast, the addition of seeds of the short-lived polymorph leads to different outcomes depending on the milling conditions.

Under LAG conditions, the seeds of the short-lived polymorph are rapidly consumed, forming the corresponding homodimers via disulfide bond breaking and bond reforming. These homodimers then undergo the typical sequence of induction, reaction, and steady state, ultimately yielding the persistent polymorph.

Under NG conditions, the added seeds of the short-lived polymorph instead slowly transform into the persistent polymorph through direct polymorphic interconversion until they are fully consumed, without involving disulfide bond breaking or formation, ultimately yielding the persistent polymorph.

Thus, direct polymorph interconversion can be achieved under both NG and LAG conditions in the absence of DBU, provided

View Article Online
DOI: 10.1039/D6CP00448B

that the milling conditions are adjusted to favour the desired polymorph. This confirms that polymorphic transformations can proceed independently of disulfide exchange and that DBU specifically enables access to exchange-mediated, sequential pathways via the corresponding homodimers.[51]

12 Crystal size matters!

Crystals can be stabilised either by their bulk or by their surface. At large sizes—micrometer, millimeter, or even centimeter scale, bulk stabilisation dominates, and conventional thermodynamic phase diagrams can reliably predict relative stability. This situation typically occurs during crystallisation from solution or under slurry conditions (Figure 28b).

However, as crystals are reduced in size by ball milling, surface effects begin to dominate. At the nanoscale, surface energy becomes the controlling factor, and the relative stability of the crystal can be influenced by the type and volume of solvent used under LAG conditions (Figure 28a). Depending on these conditions, multiple surface-stabilised polymorphs can form.[10] Importantly, nanocrystals are not thermodynamically stable, and their growth toward bulk crystals is always favoured.

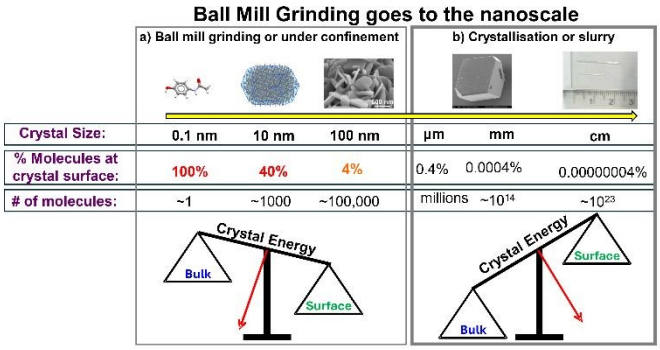

Figure 28 Effect of crystal size on polymorph formation. (a) Ball milling produces nanocrystals with significant surface contributions; (b) Solution or slurry crystallization generates µm–cm crystals where surface effects are negligible, so bulk stabilization dominates. Calculations by Aurora Cruz Cabeza.

12.1 Stabilisation of crystallites under NG conditions

The relationship between crystal size and stability has been carefully investigated.[56, 57] Navrotsky and co-workers, studying systems such as metal oxides, highlighted that "polymorphs which are metastable as micrometer-size or larger crystals can often be stabilised at the nanoscale.[58, 59] The transformation between goethite and akaganeite (FeOOH) illustrates this point clearly: as particle size decreases from the micrometer to the nanometer regime, the dramatic increase in surface area alters the relative stabilities of the polymorph.[58] This concept aligns with our kinetic NG studies of 1-2 disulfide system (Figure 20b).[51]

In our 1–2 disulfide system under NG conditions, we observe a similar size-dependent crossover, which we illustrate in Figure 29. Form A of 1–2, which is metastable at the micrometre or larger scale (the "bulk-metastable polymorph"), becomes stabilised at the nanoscale. Despite extensive attempts, Form A of 1–2 being "bulk-metastable polymorph" could not be obtained by recrystallisation, whereas Form B, the thermodynamic or bulk-stable polymorph of 1–2, was readily crystallised from a range of solvents, including ethanol, isopropanol, and acetonitrile.[10, 51]

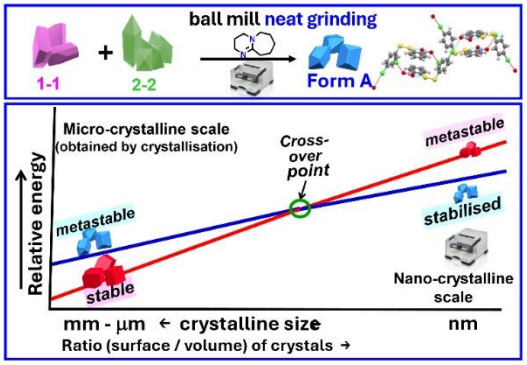

Figure 29 Stabilization of Form A of 1-2 under NG ball-milling conditions. (a) Disulfide exchange scheme under NG conditions. (b) Nanosizing-induced stability crossover: Form B, stable at µm+ sizes, becomes metastable at the nanoscale, while Form A, metastable at µm+ sizes, becomes stable at the nanoscale.[51] Adapted from Navrotsky's work on iron oxyhydroxide.[58]

In contrast, Form B of 1–2, while stable at larger, bulk-like particle sizes, becomes destabilised under NG ball-milling conditions and is never experimentally observed at the nanometre scale, as shown in Chapters 10 and 11.[10] These observations demonstrate that size-dependent surface energetics can invert the relative stability of polymorphs under mechanochemical conditions.[51]

12.2 Stabilisation of crystalline surfaces under LAG conditions

Investigating the effect of solvent on nanocrystal surfaces of metal oxides, Navrotsky concluded: "Because different solid materials (phases) have different surface energies, equilibria among them will be significantly affected by particle size."[59] Also, Navrotsky concluded: "In contact with a solvent, the particle surfaces are solvated. A key point is the importance of particle size and hydration in determining the energetics and in stabilising, at the nanoscale, phases metastable in the bulk."[58] Navrotsky also noted that "the high surface-to-volume ratio in nanomaterials makes them much more reactive toward their surroundings than bulk materials."[59]

View Article Online
DOI: 10.1039/D6CP00448B

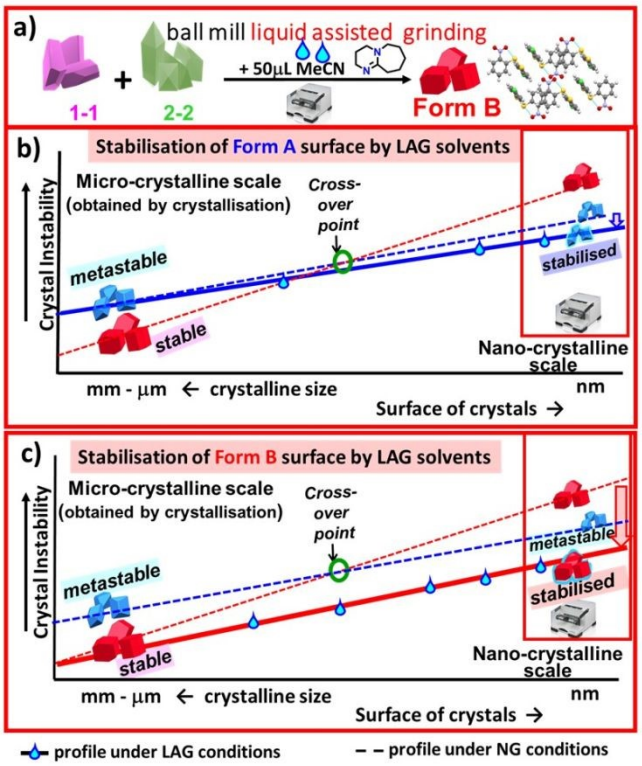

Figure 30 Surface-driven stabilization of Form B under LAG conditions. Inspired by Navrotsky's work on (FeOOH).[59] a) Reaction scheme: Form B of 1-2 is formed under LAG. b) LAG solvents provide minimal nanoscale surface stabilization to Form A. c) Strong nanoscale surface stabilization of Form B by LAG solvents renders it more stable than Form A, explaining its exclusive formation under LAG conditions.[51]

This interpretation is fully consistent with the kinetic LAG data shown in Figure 20c and explains why Form B is the polymorph stabilised under LAG conditions.[51]

We hypothesise that these thermodynamic principles, established for the Goethite–Akaganeite transformation (FeOOH) in the presence of water, are directly relevant to our ball-milling LAG experiments of the 1-2 disulfide system.

Figure 30 shows how we interpret Navrotsky's findings in the context of the 1-2 system under LAG conditions. In Figure 29, we proposed that Form A becomes stabilised under NG conditions because of nanoscale surface effects. Under LAG conditions, however, the added solvent solvates and stabilises the particle surfaces differently. In this environment, the surfaces of Form B (Figure 30c) are preferentially stabilised over those of Form A (Figure 30b). As a result, only Form B persists under LAG conditions, whereas Form A does not form.

These predictions align well with our experimental Scherrer crystallite sizes: Form A of 1-2 is typically around 40 nm, and Form B of 1-2 falls in the 60–80 nm range, as shown in Figure 32.[10]

The same trends was obtained when the relative energies of Forms A and B was calculated at nanoscale dimensions and in the presence of solvent, as shown in Figure 31.[10] The calculations reveal a crossover at approximately 40 nm: below this size, Form A is more stable than Form B, while above 40 nm the stability reverses, and Form B becomes the more stable form (Figure 31a).[10]

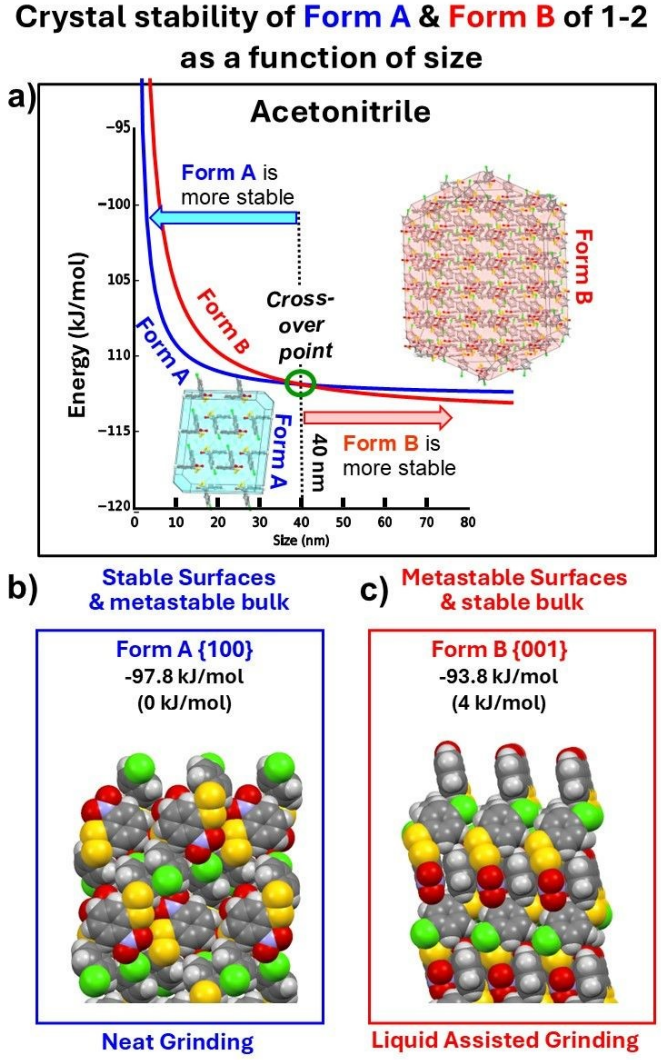

Figure 31 Size-dependent polymorph stability. a) Calculated stability crossover at ~40 nm: Form A of 1-2 is favoured <40 nm, Form B of 1-2 >40 nm. b) Form A of 1-2: stable surface, metastable bulk. c) Form B of 1-2: metastable surface, stable bulk.[10] Adapted from ref. 10 with permission from The Royal Society of Chemistry

Bulk and surface energies were calculated using acetonitrile as the LAG solvent (Figure 31c). Form A was found to have a stable surface but a metastable bulk (Figure 31b) obtained under NG conditions, whereas Form B has a metastable surface, but a stable bulk obtained under LAG (acetonitrile) conditions. (Figure 31b) and by crystallisation.[10]

13 Polymorph interconversions

We highlight diverse examples of polymorph formation and interconversion by ball milling, ranging from disulfide exchange in the presence of DBU, which involves bond breaking and reforming (Sections 13.1–13.2), to transformations of disulfide crystals that occur without bond rearrangement (Sections 13.3–13.5). The discussion is extended to polymorph interconversion in single-component systems (Section 13.6) and cocrystals

View Article Online
DOI: 10.1039/D6CP01418B

(Section 13.7), illustrating the broad scope of ball milling polymorphism.

13.1 Polymorph interconversion between Form A and Form B of 1-2 in presence of catalyst

Based on the kinetic findings in Figure 20, we reasoned that if Form A is obtained exclusively under NG conditions at steady-state (Figure 20b), and Form B is obtained exclusively under LAG conditions at steady-state (Figure 20c), then the two polymorphs should be interconvertible simply by applying the milling conditions that favour each form and milling to steady-state.[51]

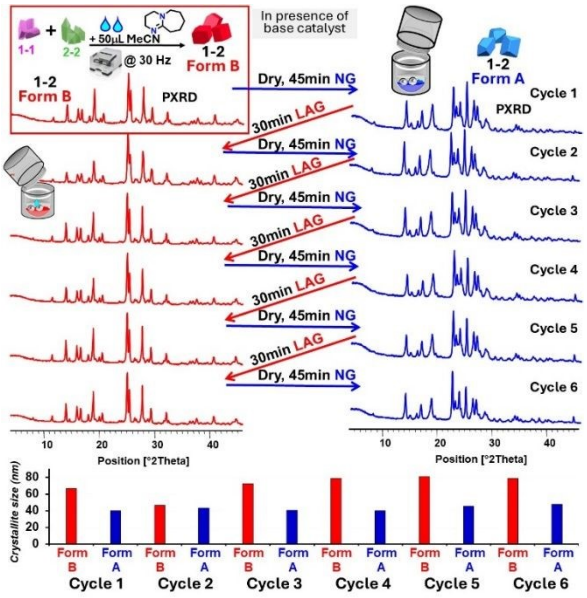

Figure 32 Ball-mill interconversion of Forms A and B of 1-2. Initial Form B of 1-2 is dried and converted to Form A by NG milling (45 min, 30 Hz). Form A is reconverted to Form B by LAG with 50 µL MeCN (30 min, 30 Hz), and the cycle is repeated six times. Milled Form B yields 60–80 nm crystallites; milled Form A yields ~40 nm crystallites.[10] Adapted from ref. 10 with permission from The Royal Society of Chemistry.

This hypothesis was tested experimentally, and the results fully matched our expectations (Figure 32). Form B was first prepared from an equimolar mixture of 1-1 and 2-2 under LAG conditions (50 µL MeCN) in the presence of DBU and milled to steady-state (30 minutes at 30 Hz). After drying, this Form B powder was milled under NG conditions (45 minutes), resulting in complete conversion to Form A. Reversing the process, milling Form A under LAG conditions, restored Form B. Subsequent drying of Form B followed by milling under NG conditions again regenerated Form A. This interconversion cycle was repeated six times in the same milling jar, as shown in Figure 32.[10]

13.2 Polymorph interconversion between Form A and Form B of 1-3 in presence of catalyst

We next extended the polymorph-interconversion strategy described in Section 13.1 to the 1–3 disulfide system. As anticipated, the steady-state polymorph-interconversion behaviour of the 1–3 system (Figure 33) closely mirrored the polymorph distributions observed in the earlier kinetic studies conducted in the presence of DBU (Section 11.2, Figure 21) at steady-state.[53] Because disulfide bonds continuously break and reform during milling, the system evolves toward a steady-state composition dictated by the applied milling conditions.

The experiment was initiated by preparing Form B of 1-3 via milling equimolar amounts of 1-1 and 3-3 in the presence of DBU under LAG conditions (50 µL MeCN, 45 minutes, 30 Hz), affording Form B of 1–3 in >99 mol%. After drying, this Form B material was milled under NG conditions (3h, 30 Hz), resulting in transformation to Form A of 1–3 at approximately 85 mol%.

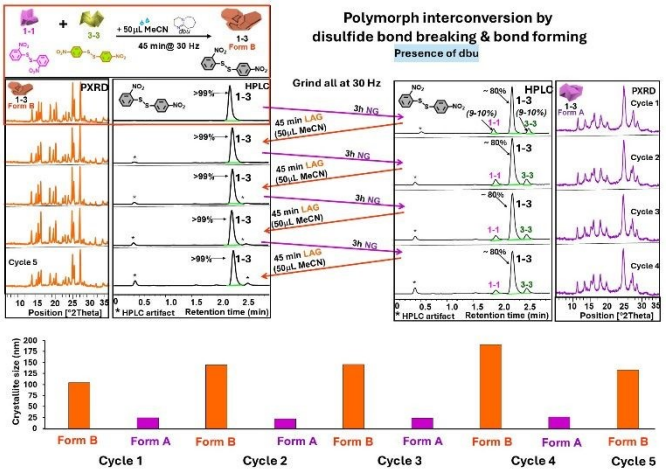

Figure 33 Polymorph interconversion of 1-3 under NG and LAG milling. Initial Form B of 1-3 (>99 mol% by HPLC) is dried and converted to Form A of 1-3 at~80 mol% by NG (3 h, 30 Hz). Form A of 1-3 is reconverted to Form B of 1-3 at >99 mol% by LAG with 50 µL MeCN (45 min, 30 Hz). The cycle is repeated five times. Crystallite sizes: Form B of 1-3=110–180 nm; Form A of 1-3=~30 nm.[53] Adapted with permission from Ref [53]. Copyright [2021] Wiley.

Conversely, milling Form A under LAG conditions (50 µL MeCN, 45 minutes, 30 Hz) quantitatively regenerated Form B (>99 mol%). These NG/LAG interconversions were repeated five times in the same milling jar, as shown in Figure 33.[53]

To more clearly illustrate the reproducibility and composition of the polymorphs formed at steady-state, Figure 33 also presents HPLC analyses collected over five NG/LAG turnover cycles. These data demonstrate that the two polymorphs reproducibly reach distinct steady-state compositions depending on the milling conditions applied: approximately 85 mol% for Form A and >99 mol% for Form B. Consistent with earlier observations on the crystallite sizes of milled polymorphs, Form B exhibits crystallite sizes above 100 nm, whereas Form A forms significantly smaller crystallites of approximately 30 nm.[53]

13.3 Polymorph interconversion between Form A and Form B of 1-3 in the absence of catalyst

In the absence of DBU, polymorph interconversion in the 1–3 system (Figure 34) differs markedly from that observed in its presence (Figure 33). Because no disulfide bond breaking can occur without DBU, the overall chemical composition is conserved throughout the polymorph-interconversion

View Article Online
DOI: 10.1039/D5CP04185

experiments. Consequently, these experiments are initiated from pure crystals of Form B of 1–3 (100 mol%) that are completely free of DBU traces, to avoid any bond-breaking or bond-forming processes during milling.

Pure Form B of 1–3 was prepared by first milling equimolar amounts of 1–1 and 3–3 on gram scale in the presence of DBU under LAG conditions with MeCN to obtain Form B quantitatively (>99 mol%). This material was then recrystallised from MeCN, with the solvent containing enough TFA to neutralise residual DBU and thereby prevent scrambling into a statistical mixture of homodimers and heterodimer. The resulting crystals were carefully rinsed to remove all traces of DBU and TFA, and only the first crop confirmed by HPLC to be pure Form B of 1–3 was used for subsequent polymorph-interconversion experiments.

Pure Form B of 1–3 (200 mg) was milled under NG conditions (3 h, 30 Hz), resulting in quantitative conversion to Form A of 1–3. Subsequent milling under LAG conditions (50 µL MeCN, 45 minutes, 30 Hz) converted Form A back to Form B of 1–3. Four consecutive polymorph turnover cycles were performed, demonstrating consistent and fully reversible interconversion between the two polymorphs while maintaining the pure composition as per HPLC analysis.

Consistent with earlier observations, Form A of 1–3 forms nanocrystalline material with crystallite sizes of approximately 30 nm, whereas Form B of 1–3 consists of larger crystallites in the range of 60–120 nm.[53]

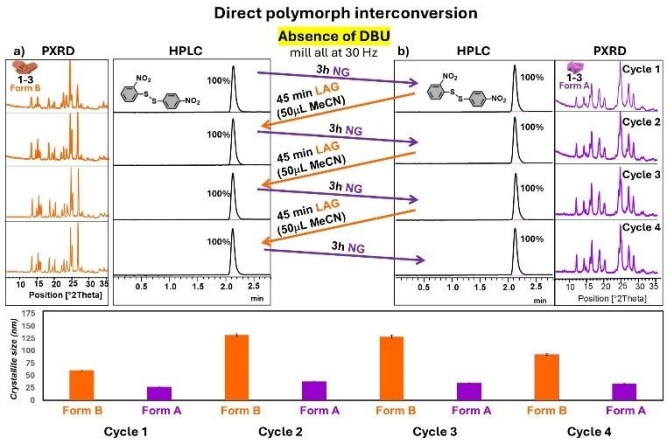

Figure 34: DBU-free polymorph interconversion of 1-3 by ball milling. Pure Form B crystals of 1-3 (100 mol%, recrystallised from MeCN and rinsed to remove traces of DBU) is converted to Form A by NG milling (3 h, 30 Hz) and back to Form B by LAG (50 µL MeCN, 45 minutes, 30 Hz). The cycle is repeated four times, with 100 mol% yield for both polymorphs (HPLC). Crystallite sizes: Form B of 1-3=60–120 nm; Form A of 1-3= 20–30 nm.[53] Adapted with permission from Ref [53]. Copyright [2021] Wiley.

13.4 Polymorph interconversion between Form A and Form B of 1-2 in the absence of catalyst

We attempted to achieve solid–solid polymorph interconversion between Form B and Form A of the 1–2 disulfide system using an approach analogous to that successfully applied to the 1–3 disulfide system (Section 13.3), starting from pure crystals of Form B of 1–2 free of DBU. Despite numerous attempts over several years, this polymorph interconversion was not successful. Only later did we establish that interconversion between Form A and Form B of 1–2 requires the presence of at least 1.5 mol% of the homodimer (2-$NO_2PhS)_2$ (1–1), which we hypothesise acts as a templating agent, as discussed in Section 13.5.[60]

13.5 Templated polymorph interconversion

We discovered a new polymorph of 1-2, Form C, by milling pure crystals of Form B under LAG conditions with water.[60]

The crystals of Form B of 1-2 were obtained from recrystallisation of high yielding Form A or Form B, as once the crystals went into solution, its crystalline precedence did not matter, and it became 1-2. 1-2 was recrystallised from various solvents such as MeCN, MeOH, EtOH and IPA containing TFA to neutralise the DBU present in the powder, to avoid scrambling. Form B of 1-2, the thermodynamic stable bulk polymorph was obtained and extensively washed to remove any traces of DBU and TFA, so that milling would proceed via direct modification of crystal lattices avoiding disulfide bond breaking and reforming.

We found on intensive testing (see Section 13.4) that at least 1.5 mol% of the homodimer 1-1 was required for these transformations; in its absence no polymorph transformation took place. This suggest that 1-1 may act as a template.

In the presence of 1.5 mol% 1–1, 300 mg of Form B of 1–2 could be quantitatively transformed to Form C under LAG conditions (75 µL H_2O, 90 minutes, 30 Hz), then to Form A under NG conditions (90 minutes, 30 Hz), and back to Form B under LAG conditions (75 µL MeCN, 45 minutes, 30 Hz) (Figure 35a). The transformations could also be performed in reverse order: Form B of 1–2 was converted to Form A under NG conditions (3 h 30 minutes, 30 Hz), then to Form C under LAG conditions (75 µL H_2O, 90 minutes, 30 Hz), and finally reverted to Form B under LAG conditions (75 µL MeCN, 45 minutes, 30 Hz) (Figure 35b). Each sequence was repeated twice. The three polymorphs exhibited distinct crystallite sizes: Form A, 40–60 nm; Form C, 70–90 nm; and Form B, 120–140 nm (Figure 35).[60]

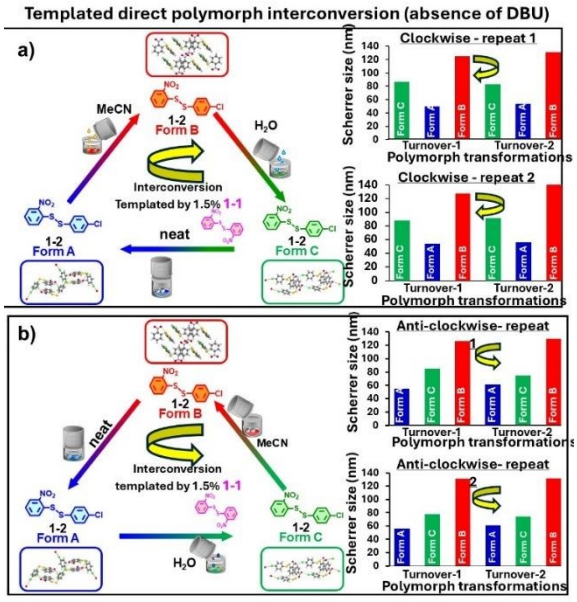

View Article Online
DOI: 10.1039/D6CP00448B

Figure 35 Three-polymorph interconversion of 1-2 under ball milling. ≥1.5 mol% 1-1 enables transformations, likely acting as a template. a) Clockwise: Form B → Form C → Form A → Form B → Form C → Form A → Form B. b) Anticlockwise: Form B → Form A → Form C → Form B → Form A → Form C → Form B. Form A forms by NG; Form C by LAG with water; Form B by LAG with MeCN. Crystallite sizes: Form A= 40–60 nm; Form C= 70–90 nm; Form B= 120–140 nm.[60] Adapted from ref. 60 with permission from The Royal Society of Chemistry.

13.6 Polymorph interconversion of single component molecular crystal by milling

We next tested whether polymorph interconversions could be observed in non-disulfide systems.

We studied several published examples of milled polymorphs: γ- and α-D-sorbitol (Figure 36a,b), [61, 62] α- and τ-chlorpropamide (CPA) (Figure 36c,d),[63] ε- and α-N-acetyl-1-phenylalanine amide (Ac-Phe-NH_2) (Figure 36e,f),[64] and Caffeine Form I and Form II (Figure 36g,h).[65] In all cases, the polymorphs could be directly transformed into each other via modification of their crystal lattices. Once the milling conditions favouring the formation of each specific polymorph were developed, polymorph interconversions were reproducible across two cycles for each system.[12, 13]

For all these examples, milling was carried out well beyond the minimum milling time required under NG and LAG conditions to achieve steady-state. Continuous milling suppressed spontaneous crystallite growth while maintaining steady-state, which improved crystallinity and enhanced PXRD resolution. As M. Descamps noted, "After a long enough milling, the Bragg peaks of the appearing new form progressively become very sharp. This shows that milling is able at that time to promote a total reconstruction of the new long-range order on a large microstructural scale."[61]

Polymorph transformation of D-Sorbitol as in Figure 36a,b from Form γ → Form α is achieved by milling over 8 h at 30 Hz under NG conditions, and from Form α → Form γ, by milling over 1 hour at 30 Hz under LAG conditions (50 μL MeCN). The crystallite sizes: Form α=120–150 nm, Form γ=70–80 nm.[13]

Polymorph transformation of chlorpropamide (CPA) as in Figure 36c,d from Form α →Form η is achieved by milling under NG conditions over 6h at 30 Hz,[12] and from Form η → Form α, by milling over 1 hour at 30 Hz under LAG conditions (50 μL MeCN). The crystallite sizes: Form α=300–350 nm, Form η= 50–100 nm.[13]

Polymorph transformation of N-acetyl-1-phenylalanine amide (Ac-Phe-NH_2) as in Figure 36e,f from Form ε → Form α is achieved by milling over 8 h at 30 Hz under NG conditions, and from Form α → Form ε, by milling over 1 hour at 30 Hz under LAG conditions (100 μL H_2O). The crystallite sizes: Form α=30–50 nm, Form ε=130–150 nm.[13]

Polymorph transformation of Caffeine as in Figure 36g,h from Form II → Form I is achieved by milling over 45 minutes at 30 Hz under NG conditions, and from Form I → Form II, by milling over 15 minutes at 30 Hz under LAG conditions (50 μL MeCN). The crystallite sizes: Form I=~50 nm, Form II =100–120 nm.[13]

Freshly prepared experiments intended for SEM studies, are included in Ac-Phe-NH_2 (Figure 36e,f) and Caffeine (Figure 36g,h) to demonstrate reproducibility of polymorph formation and interconversion.[13]

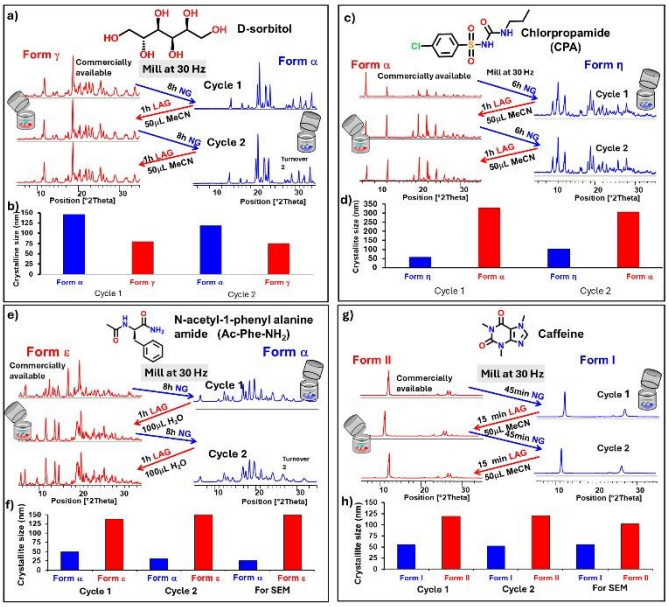

Figure 36 Milling conditions to steady-state for polymorph formation and interconversion and their corresponding crystallite size; a) & b) D-Sorbitol: Form γ ↔ Form α (NG/LAG with MeCN); c) & d) chlorpropamide (CPA): Form α ↔ Form η (NG/LAG with MeCN); e) & f) N-acetyl-1-phenylalanine amide (Ac-Phe-NH_2): Form ε ↔ Form α (NG/LAG with H_2O); g) & h); Caffeine: Form II ↔ Form I (NG/LAG with MeCN). Polymorph formation Ac-Phe-NH_2 and caffeine intended for SEM measurements are included to further demonstrate reproducibility.[13] Adapted from ref. 13 with permission from The Royal Society of Chemistry.

13.7 Polymorph interconversion of multiple component molecular crystals by milling

The next challenge was to apply polymorph interconversion by ball milling to multicomponent molecular crystals. We investigated two cases: 1:1 theophylline:benzamide cocrystal (Section 13.7.1) and 1:1 melamine:barbiturate cocrystal (Section 13.7.2).

13.7.1 1:1 theophylline:benzamide cocrystal

We investigated the 1:1 theophylline : benzamide (tp:ba) cocrystal, where Form I of 1:1 tp:ba, obtained under NG conditions and Form II of 1:1 tp:ba, obtained under LAG conditions with water, was previously reported by Emmerling et al.[42]

View Article Online
DOI: 10.1039/D6CP00448B

The goal of our investigation was to transform Form I to Form II under LAG conditions with water and Form II to Form I under NG conditions, always milling to steady-state.

We followed the experimental setup from Emmerling et al., using a 1 g loading, two milling balls of 10 mm diameter and 250 µL water for the LAG transformation and milling was performed on the MM400 at 30 Hz. We modified the published protocol by using a 14.5 mL instead of 10 mL milling jar.

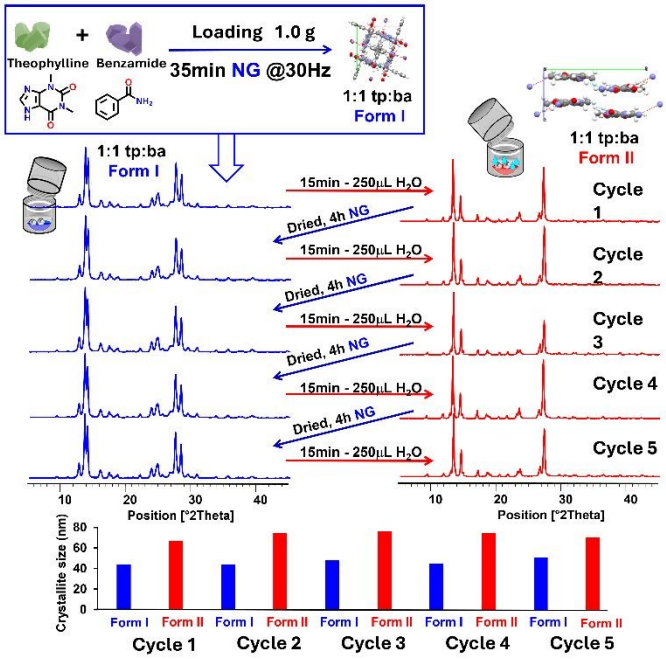

Figure 37 Polymorph interconversion of 1:1 tp:ba cocrystals by ball milling at 1 g scale. Form I to Form II (LAG with 250 µL H_2O, 15 min, 30 Hz). Form II is dried and reconverted to Form I (NG, 4 h, 30 Hz). Five turnover cycles performed. Crystallite sizes: Form I= ~40 nm; Form II= 60–80 nm.[10] Adapted from ref. 10 with permission from The Royal Society of Chemistry.

As with the published data from Emmerling et al, polymorph interconversion from Form I to Form II was achieved by LAG with 250 µL water milling over 15 minutes at 30 Hz; the transformation of Form II to Form I was achieved by milling over 4 h at 30 Hz under NG conditions. Figure 37 summarises the data of 5 turnover cycles.[10]

Form I was initially prepared by ball mill NG from an equimolar mixture of anhydrous theophylline and benzamide. Milled Form I has a crystallite size of around 40 nm, while milled Form II consistently has a crystallite size of 60–80 nm.[10]

13.7.2 1:1 Melamine Barbiturate cocrystal

Another example of polymorph interconversion between cocrystals is observed in the 1:1 ME:BA system, where ME is N,N'-bis(4-tert-butylphenyl)melamine and BA is diethyl barbiturate (Figure 38). The Whitesides group previously reported a rosette polymorph of the 1:1 ME:BA cocrystal obtained by crystallisation from a toluene/isopropyl alcohol mixture (1:1 v/v). They further proposed that two additional polymorphs—a linear tape and a crinkled tape—should be feasible; however, despite extensive crystallisation efforts, these forms could not be isolated.[66]

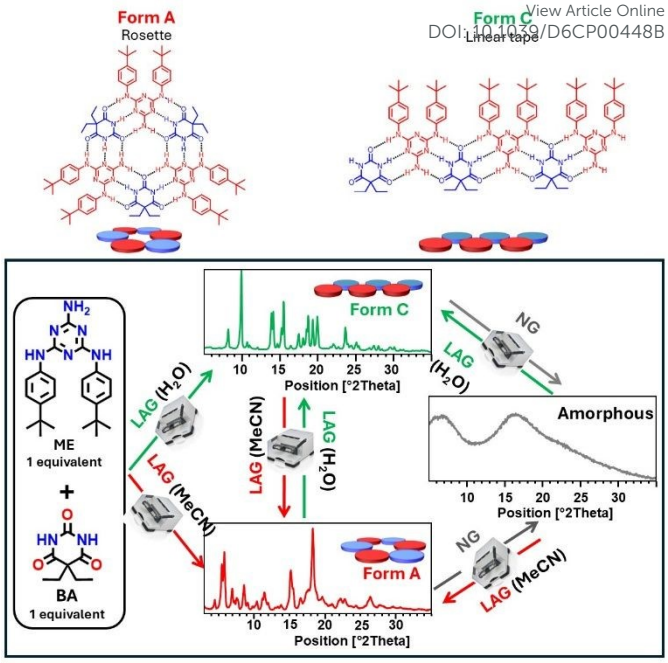

Figure 38 Polymorph interconversion of 1:1 ME:BA cocrystals by ball milling. NG milling of 1:1 ME:BA consistently yields the amorphous form. LAG with MeCN produces Form A (rosette), whereas LAG with water produces Form C (linear tape). All three forms can be obtained directly by milling an equimolar mixture of ME and BA to steady-state.[67] Adapted from ref. 67 with permission from The Royal Society of Chemistry.

Using ball-milling methods, we obtained the 1:1 ME:BA rosette polymorph (Form A) by milling equimolar amounts of ME and BA for 1 h at 30 Hz under LAG conditions with 50 µL MeCN.[67] When the same equimolar mixture was milled with 50 µL water for 3 h at 30 Hz, an unpublished polymorph was obtained. This form, designated Form C, was structurally identified as a linear tape arrangement. Milling equimolar amounts of the coformers for 1–3 h at 30 Hz to reach steady-state under NG conditions resulted in an amorphous phase. The crystal structures of Form A (rosette) and Form C (linear tape) are shown in Figure 38.[67]

Form C could be transformed back into Form A either by milling for 3 h at 30 Hz with 20 µL MeCN or to the amorphous form through NG milling for 6 h at 30 Hz. Conversely, Form C was regenerated when Form A was milled for 1 h at 30 Hz under LAG conditions with water (100 µL), or when the amorphous phase was milled for 2 h at 30 Hz under LAG conditions with water (50 µL). The amorphous form could likewise be regenerated by milling either Form A or Form C for 6 h at 30 Hz under NG conditions. Form A could be regenerated from the amorphous phase when it was milled for 2 h at 30 Hz under LAG conditions (50µL MeCN).

It should be noted that milling was always carried out for durations exceeding those strictly required to reach steady-state, and that solvent volumes sufficient to ensure quantitative formation of the desired polymorph were added in excess of the minimum necessary.[67] The use of excess solvent does not pose any issues, as explained later in Section 14.

These polymorph interconversions are illustrated in Figure 38. Overall, all three solid forms of the 1:1 ME:BA system—Form A (rosette), Form C (linear tape), and the amorphous phase—can

be reversibly interconverted through ball milling under conditions that favour their respective formation.[67]

13.8 Lessons learned

Ball milling demonstrates the dynamic interconversion of polymorphs, either through bond breaking and reforming in the presence of a catalyst (e.g., disulfides with DBU) or via direct lattice modification in its absence. Turnover cycles can be performed repeatedly on the same powder, for single-component crystals, multicomponent cocrystals, and even systems requiring a templating molecule as far as the milling conditions that favours the formation of a desired polymorphs are applied.

Typically, NG yields the smallest crystallites, LAG the largest, with exceptions such as α-D-sorbitol.

These findings highlight how milling conditions control both polymorph formation and crystallite size, providing a predictable and reproducible approach to mechanochemical polymorph control.

14 Effect of volume and type of solvent loaded on the outcome of ball LAG reactions

We sought to address a fundamental question in LAG: how does the amount of added solvent influence polymorph selection at steady-state? Does the expected LAG polymorph form reliably across different solvent types and volumes?

Throughout this work, disulfide-exchange reactions of the 1–2 model system were conducted using a fixed solvent volume (50 µL MeCN per 200 mg),[10, 41, 51] while polymorphic transformation of the 1:1 tp:ba cocrystal model system employed 250 µL of water per 1 g loading[10, 68]. To systematically probe the role of solvent quantity in both systems, we introduced a framework we term “steady-state solvent curves”, in which reactions or transformations are milled for sufficiently long durations to ensure attainment of steady-state.

Steady-state solvent curves were constructed by initiating experiments under NG conditions, followed by experiments milling with progressively increasing volumes of a selected solvent until the LAG polymorph was obtained quantitatively. Two characteristic solvent thresholds are defined: V_o, below which no LAG polymorph forms, and V_{100}, the minimum solvent volume required to obtain the LAG polymorph quantitatively under the prevailing chemistry and milling conditions.[69]

Section 14.1 presents steady-state solvent curves for the disulfide-exchange system, while Section 14.2 applies this approach to polymorph interconversion in the tp:ba cocrystal system.

14.1 Steady-state solvent milling curves for disulfide exchange ball mill reactions

Steady-state solvent curves were constructed for the 1–2 disulfide exchange reaction by milling equimolar mixtures of 1–1 and 2–2 (200 mg loading) in the presence of DBU to steady-state using progressively increasing volumes of LAG solvent. For each solvent, the steady-state fraction of Form B was quantified by PXRD/Rietveld analysis and plotted as a function of solvent volume, revealing a characteristic sigmoidal dependence in all cases.[10]

For acetonitrile (Figure 39), a sharp transition was observed: Form A was obtained exclusively up to 21 µL (V_o), while quantitative formation of Form B occurred abruptly at 22 µL (V_{100}) and persisted at higher solvent volumes.[10]

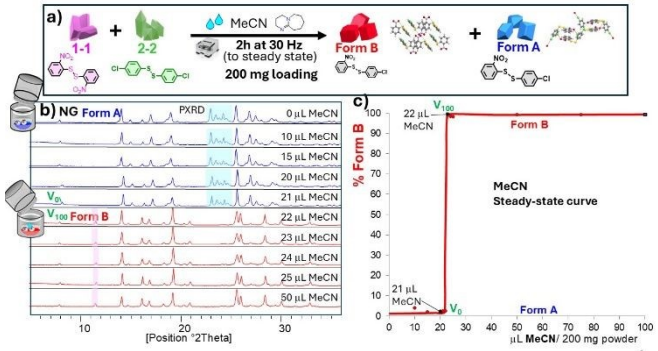

Figure 39 MeCN steady-state solvent curve of 1–2 disulfide polymorphs. (a) Reaction scheme. (b) PXRD patterns collected during LAG milling (MeCN) of 1–1 + 2–2 in the presence of DBU, showing that milling for 2 h at 30 Hz reaches a steady-state. Form A is obtained at ≤21 µL MeCN, while Form B is obtained at ≥22 µL MeCN. (c) Formation profile of Form B of 1–2 as a function of MeCN volume added (mol% Form B vs µL MeCN per 200 mg of powder). An abrupt switch between Form A and Form B is observed at 22 µL, corresponding to the onset value V_{100} for MeCN.[10] Adapted from ref. 10 with permission from The Royal Society of Chemistry

In contrast, ethyl acetate (EtOAc) exhibited a much shallower sigmoidal profile, with Form A persisting up to 20 µL (V_o), mixed Form A/Form B compositions between 23–28 µL, and quantitative formation of Form B only at 30 µL (V_{100}).

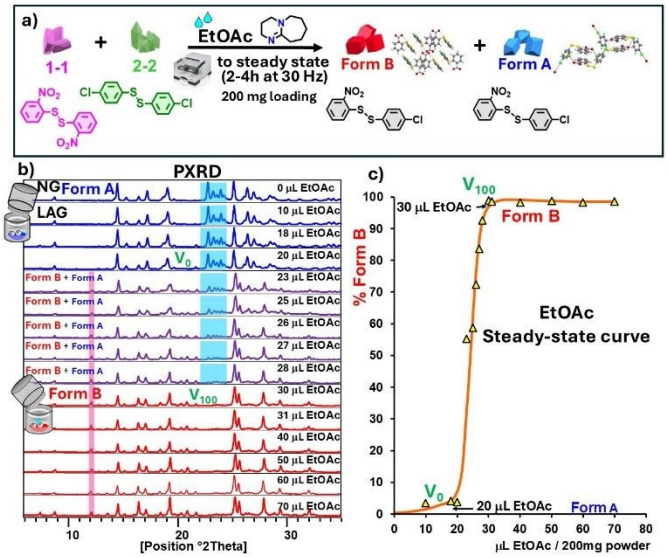

Figure 40 EtOAc steady-state solvent curve of 1–2 disulfide polymorphs. (a) Reaction scheme. (b) PXRD patterns collected during LAG milling (EtOAc) of 1–1 + 2–2 in the presence of DBU, showing that milling for 2–4 h at 30 Hz reaches steady-state. Form A is obtained at ≤20 µL EtOAc (V_o = 20 µL), mixed Form A/Form B compositions between 23–28 µL, while Form B is obtained at ≥30 µL EtOAc (V_{100} = 30 µL). (c) Formation profile of Form B of 1–2 as a function of EtOAc volume added (mol% Form B vs µL EtOAc per

View Article Online
DOI: 10.1039/D6CP00448B

200 mg of powder).[10] Adapted from ref. 10 with permission from The Royal Society of Chemistry.

Compilation of steady-state solvent curves for 15 solvents reveals that each solvent is characterised by distinct V_o and V_{100} values. Aprotic solvents such as acetone and acetonitrile show sharp, well-defined transitions, whereas solvents including DMF, $CHCl_3$, and EtOAc display broad mixed-phase regimes. Alcohols (MeOH, EtOH, IPA) and DMSO require substantially higher solvent volumes (>45 µL per 200 mg) to reach V_{100}, while highly hydrophilic (water) or highly lipophilic solvents (benzene, toluene, cyclohexane) yield exclusively Form A across the entire volume range investigated.[10, 39]

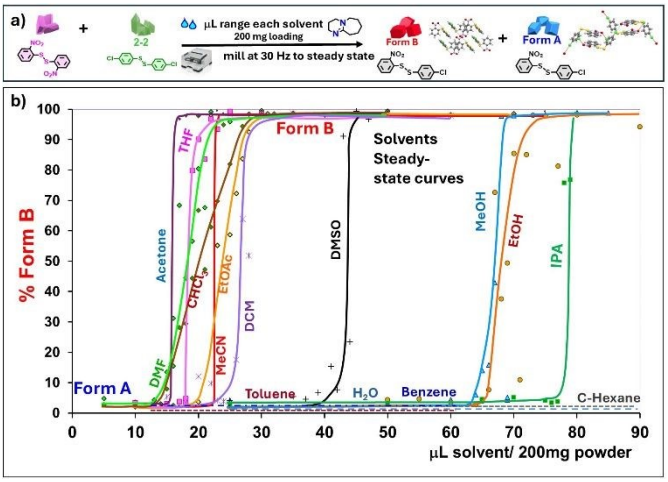

Figure 41 Solvent steady-state curve profiles for 1–2 disulfide polymorphs. (a) Reaction scheme. (b) LAG milling of 1–1 + 2–2 with DBU at 30 Hz, showing the mol% of Form B as a function of solvent volume added (µL solvent per 200 mg of powder) for 15 different solvents. The profiles illustrate solvent-dependent steady-state formation of Form B, with each solvent exhibiting a distinct onset value V_{100} and characteristic slope. Each data point in each solvent profile represents an independent experiment milled to steady-state.[10] Adapted from ref. 10 with permission from The Royal Society of Chemistry.

14.2 Steady-state solvent milling curves for 1:1 tp:ba cocrystal polymorphs

To test whether the concept of steady-state solvent curves is transferable beyond reactive systems, we applied the same approach to a multicomponent molecular crystal, namely the 1:1 tp:ba cocrystal discussed in Section 13.7.1.

Using pre-formed Form I (1g loading) as the starting material enabled direct interrogation of polymorphic outcomes, avoiding complications associated with cocrystal formation kinetics. In all cases, milling was conducted for sufficiently long durations to ensure attainment of steady-state.

Steady-state solvent curves constructed using MeCN, chloroform, water, and a total of 15 solvents reveal solvent-specific volume thresholds for transformation from Form I to Form II.[68]

With MeCN (Figure 42), a sharp transition is observed for the steady-state solvent curve: Form I persist under NG conditions and up to 7 µL MeCN (V_o) while quantitative conversion to Form II occurs abruptly at 8 µL (V_{100}) and remains complete at higher solvent volumes. This behaviour closely mirrors the sharp solvent-volume transition observed for the disulfide system using MeCN.

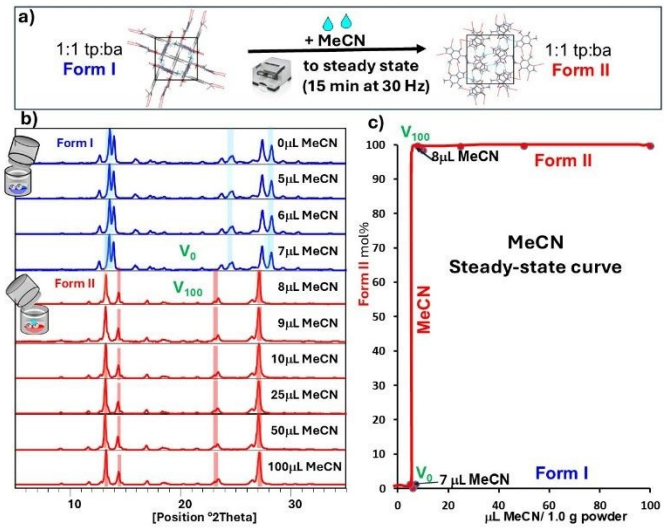

Figure 42 MeCN steady-state solvent curve of 1:1 tp:ba cocrystal polymorphs. (a) Reaction scheme. (b) PXRD patterns collected during LAG milling (MeCN) of 1 g of Form I (15 min, 30 Hz), showing that milling reaches a steady-state. It yields Form I at ≤7 µL MeCN (V_0 = 7 µL) and quantitative Form II at ≥8 µL MeCN (V_{100} = 8 µL). (c) Formation profile of Form II as a function of MeCN volume added (mol% Form II vs µL MeCN per 1 g of powder). Each data point represents an independent experiment milled to steady-state.[68] Adapted from Ref 68 with permission from *JACS*, 2018, 140, 17051-17059, Copyright {2018} American Chemical Society.

In contrast, chloroform (Figure 43) produces a broad sigmoidal profile for the steady-state solvent curve, with mixed Form I/Form II compositions appearing above 33 µL (V_o) and quantitative formation of Form II achieved only at higher solvent volumes (V_{100} ≈ 35 µL).

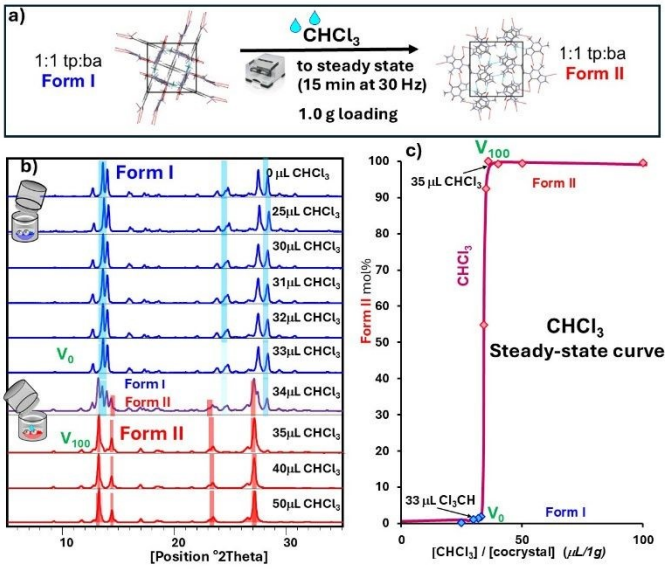

Figure 43 $CHCl_3$ steady-state solvent curve of 1:1 tp:ba cocrystal polymorphs. (a) NG and LAG reaction scheme. (b) PXRD patterns collected during steady-state milling (15 minutes, 30 Hz) with increasing $CHCl_3$ volume, showing that milling reaches steady-state. It yields Form I at ≤33 µL $CHCl_3$ (V_0 = 33 µL) and quantitative Form II at ≥35 µL $CHCl_3$ (V_{100} = 35 µL). (c) Formation profile of Form II as a function of $CHCl_3$ volume added (mol% Form II vs µL $CHCl_3$ per 1 g of powder). Each data point represents an

View Article Online
DOI: 10.1039/D6CP00448B

independent experiment milled to steady-state.[68] Adapted from Ref 68 with permission from *JACS*, 2018, 140, 17051-17059, Copyright {2018} American Chemical Society.

Water exhibits intermediate behaviour, with $V_o \approx 10$ µL and V_{100} 12 µL, further demonstrating that solvent identity governs not only the onset of transformation but also the width of the mixed-phase regime.[68]

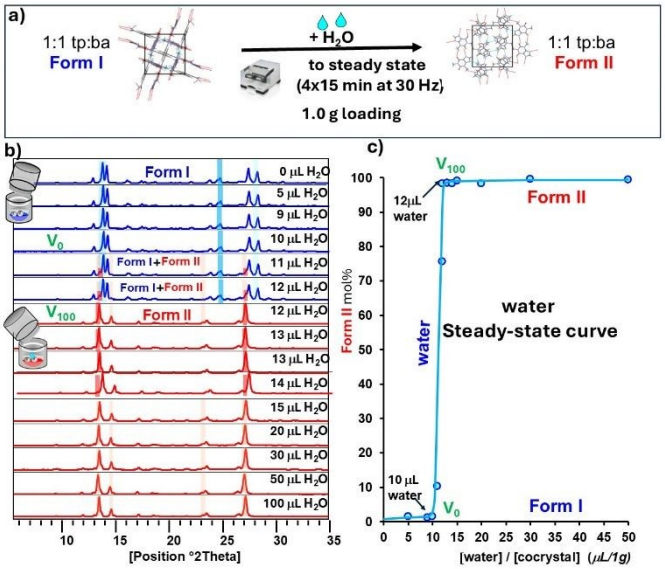

Figure 44 Water steady-state solvent curve of 1:1 tp:ba cocrystal polymorphs. (a) Reaction scheme. (b) PXRD patterns collected during LAG milling of 1 g of Form I for (4x 15 min, 30 Hz), showing that milling reaches a steady-state. It yields Form I at ≤10 µL, (V_0 = 10 µL) and quantitative Form II at ≥12 µL H_2O (V_{100} = 12 µL). c)Formation profile of Form II as a function of water volume added (mol% Form II vs µL H_2O per 1 g of powder). Each data point represents an independent experiment milled to steady-state.[68] Adapted from Ref 68 with permission from *JACS*, 2018, 140, 17051-17059, Copyright {2018} American Chemical Society.

Importantly, experiments performed with water as the LAG solvent but not milled to steady-state yield transient, time-dependent phase compositions that deviate from the sigmoidal steady-state curves. This underscores the necessity of reaching steady-state for meaningful interpretation of solvent-volume effects. Once steady-state is attained, reproducible and well-defined polymorphic outcomes are obtained (Figure 45).

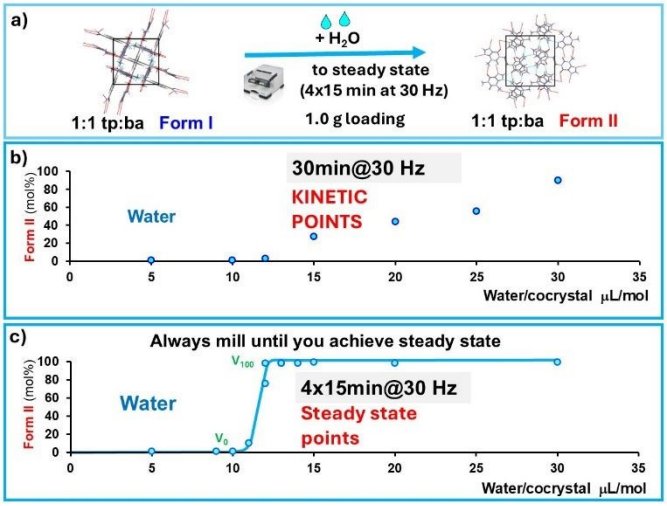

Figure 45 Effect of milling time on water steady-state solvent curves for 1:1 tp:ba cocrystals: (a) reaction scheme; (b) insufficient milling (30 minutes) yields scattered kinetic points with no steady-state curve; (c) sufficient milling (4 × 15 minutes) produces a sigmoidal solvent steady-state curve.[68] Adapted from Ref 68 with permission from *JACS*, 2018, 140, 17051-17059, Copyright {2018} American Chemical Society.

Compilation of steady-state solvent curves for all 16 solvents (Figure 46) confirms that each solvent is characterised by distinct V_o and V_{100} values for the onset and completion of Form II formation. Aprotic solvents such as acetone and acetonitrile exhibit sharp transitions, whereas solvents including nitromethane, ethyl acetate, and toluene display shallow sigmoidal behaviour. Substantially larger solvent volumes are required for IPA, benzene, $CHCl_3$, and DCM to induce transformation, while highly lipophilic solvents such as cyclohexane and perfluorodecalin fail to promote conversion to Form II under any conditions tested.[68]

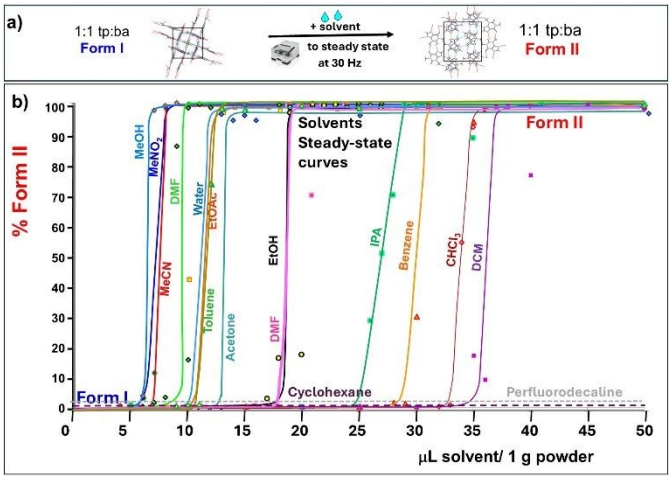

Figure 46 Steady-state solvent curves for the Form I → Form II transformation of the tp:ba cocrystal across 16 solvents. (a) Reaction scheme. (b) LAG solvent steady-state curve profiles (Form II mol% vs µL solvent per 1 g powder). Each data point represents an independent experiment milled to steady-state.[68] Adapted from Ref 68 with permission from *JACS*, 2018, 140, 17051-17059, Copyright {2018} American Chemical Society.

14.3 Lessons learned

The type and amount of solvent added during LAG can alter the surface properties of nanocrystals, shift their relative stability and thus determine which polymorph appears at steady-state.

If the volume of a given solvent is large enough to substantially modify the surface energy (identified as V_{100}), the LAG polymorph is obtained.

If the solvent amount is very low, its effect is too small and the system behaves as if no solvent were present, producing the NG polymorph instead (identified as V_0).

In intermediate cases, both polymorphs may coexist at steady-state. Increasing the solvent volume gradually increases the proportion of the LAG polymorph until a sufficiently high volume leads to its exclusive formation.

Overall, these results demonstrate that steady-state solvent milling curves provide a general and powerful framework for understanding solvent-volume-dependent polymorph selection in both reactive and multicomponent mechanochemical

View Article Online
DOI: 10.1039/D5CP00448B

systems, revealing solvent amount as a critical and non-linear control parameter.

Consistent with this discovery, LAG solvent transformation curves at steady-state have been performed by Aurora Cruz Cabeza research group with multiple solvents for the reversible interconversion of ritonavir Forms I and II.[14]

15 Achieving homogeneity on ball milling

Achieving a homogeneous product is essential in ball-milling syntheses, as heterogeneous powders cannot be reliably analysed. Powder homogeneity is governed primarily by jar loading, internal jar design, ball size and weight, and milling frequency. Accordingly, exploratory studies were conducted to ensure that in situ synchrotron milling experiments accurately reflected the true composition of the reaction mixture.

In situ X-ray diffraction (XRD) experiments require milling jars with a transparent central section. The Fritsch P23 vertical mill (Figure 2c) is well suited for this configuration. Modified jars used in this work are shown in Figures 47 and 48, and a representative jar mounted on the P23 during synchrotron operation is depicted in Figure 55.

Powder homogeneity following milling was evaluated using the disulfide-exchange 1–2 model system (Figures 47 and 48). Product distributions were quantified by HPLC, which allows direct analysis of approximately 1 mg of powder sampled from specific locations within the jar as shown at bottom of Figures 47 and 48. While HPLC can only quantify 1-2 in solution, we know that under NG conditions, 1-2 is exclusively formed as Form A. After the sample was milled, powder was collected from 9–10 positions within a three-part, 2.3 mL homemade milling jar, including the top cap, bottom cap, intermediate bottom section, and the central PMMA window, as indicated in Figures 47 and 48.

The experiment shown in Figure 47 investigated the combined effects of powder loading (25, 50, 75, and 100 mg) and milling ball diameter (single stainless-steel ball, 4–8 mm) at a milling frequency of 50 Hz. The aim was to maximise loading, powder homogeneity while avoiding caking. Reactions were performed under NG conditions using 73 mol% equimolar 1–1 and 2–2, 27 mol% of persistent polymorph Form A seeds of 1–2, and DBU. These conditions were selected such that slower reactions would not reach steady-state within 30 min, whereas faster reactions would.[55]

A 100 mg powder loading combined with a 4 mm ball resulted in caking. In contrast, 25 and 50 mg loadings produced the highest homogeneity and fastest kinetics across all ball sizes tested. For synchrotron experiments, however, a larger powder mass was required to ensure sufficient material entered the transparent central section of the jar for adequate diffraction intensity. Consequently, a loading of 100 mg combined with an 8 mm diameter milling ball was identified as the optimal compromise for in situ synchrotron measurements (Figure 47).[55]

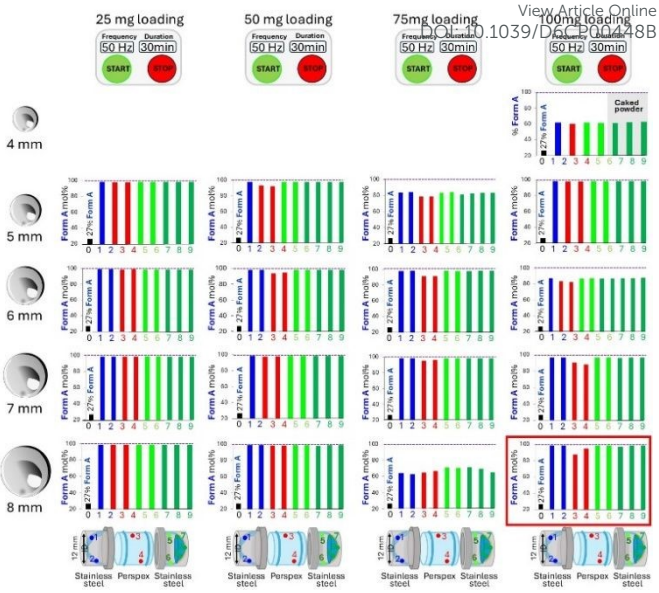

Figure 47 Effect of powder loading and milling ball diameter on reaction homogeneity in a 2.3 mL three-part milling jar for synchrotron experiments. The 2.3 mL jar with a central PMMA window is shown at the bottom, with sampling locations indicated: top cap (blue), bottom cap (green), and central PMMA window (red). Milling of the 1–2 disulfide system with DBU and 27 mol% Form A seeds of 1–2 was performed for 30 minutes under NG conditions at 50 Hz using powder loadings of 25, 50, and 100 mg and one stainless-steel ball with diameters of 4–8 mm. The setup illustrates how powder distribution and ball size influence reaction homogeneity across the jar as analysed by HPLC.[55] Adapted from ESI Ref 55 [https://www.nature.com/articles/s41467-021-26264-1] under CC BY 4.0 license.

The exploratory experiments shown in Figure 48 were designed to identify a suitable milling frequency (30–50 Hz) and ball diameter (4, 6, and 8 mm) for a 100 mg powder loading suitable for synchrotron experiments. Reactions were performed under NG conditions using equimolar 1–1 and 2–2 (100 mg total) with DBU. Milling with a 4 mm ball at 30, 40, or 50 Hz for 30 minutes consistently resulted in powder caking at the bottom cap. Consequently, for a 100 mg loading, an 8 mm diameter milling ball operated at 50 Hz was identified as the optimal compromise for in situ synchrotron measurements (Figures 47 and 48).[55]

In the HPLC analyses of the experiments shown in Figures 47 and 48, the relative content of Form B in samples taken from the central transparent section was consistently lower than in samples taken from the stainless steel caps. This is attributed to differences in surface renewal during milling: the milling ball continuously refreshes the metal cap surfaces, whereas powder adheres to the PMMA window early in the experiment due to its surface porosity. As a result, material sampled from the PMMA window is likely stratified, with earlier-deposited layers enriched in starting material and later layers enriched in product, leading to a lower apparent product content in this region.[55]

View Article Online
DOI: 10.1039/D6CP00448B

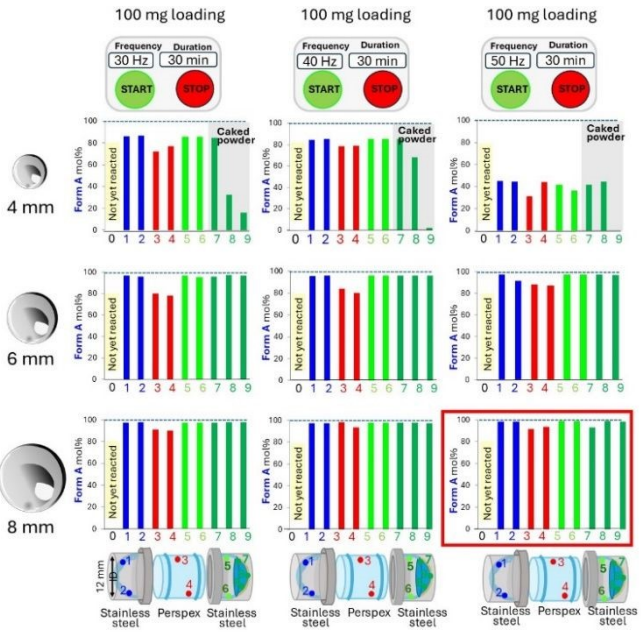

Figure 48 Optimisation of milling ball diameter and frequency for synchrotron experiments using a 100 mg powder loading. The 2.3 mL three-part jar with a central PMMA window is shown, with HPLC sampling locations indicated: top cap (blue), bottom cap (green), and central PMMA window (red). Milling of the 1–2 disulfide system with DBU under NG conditions was performed for 30 min at 30, 40, and 50 Hz using one stainless-steel balls with diameters of 4, 6, and 8 mm. The setup illustrates the effect of ball size and milling frequency on reaction progress and sample homogeneity across the jar as analysed by HPLC.55 Adapted from ESI Ref 55 [https://www.nature.com/articles/s41467-021-26264-1] under CC BY 4.0 license.

15.1 Lessons learned

Faster reaction kinetics and improved sample homogeneity are achieved at lower jar loadings and higher milling frequencies. Small milling balls (e.g. 4 mm diameter) may not adequately penetrate the powder bed; repeated impacts can instead compress the material, leading to caking and poor homogeneity. In contrast, larger balls, owing to their greater mass, penetrate the powder layer more effectively and promote improved mixing and product homogeneity throughout the jar.

16 What is the role of the induction period

All milling experiments exhibit an induction period (Figures 20, 21 and 50), the duration of which varies between systems and depends on whether milling is performed under NG or LAG conditions.[51-53] As depicted in Figure 49, we propose that during the induction stage the dominant process is mechanical fragmentation of the crystalline starting materials, affecting both single crystals and larger agglomerates. Progressive comminution leads to a reduction in particle size and the formation of defect-rich crystallites, particularly near crystal surfaces.[52, 69]

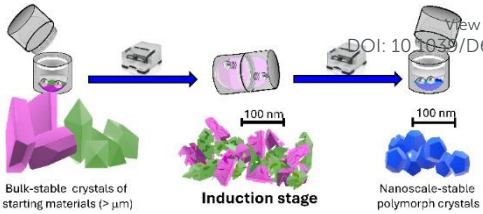

Figure 49 Proposed mechanism for the induction stage. Starting materials obtained by solution crystallisation (µm–cm scale, left) are fractured by milling into defect-rich nanocrystals (middle), enabling reaction. The final product consists of stable nanoscale polymorphs with crystallite sizes of approximately 30–200 nm (right).[52] Adapted from TOC Ref. [52, DOI: 10.3762/bjoc.15.120], under the terms of the CC BY 4.0 license.

The accumulation of mechanical energy as lattice strain and structural defects during ball milling is becoming a well-established feature of mechanochemical processes.

Mechanical fragmentation initially dissipates energy through particle size reduction, but continued milling leads to the generation of defect-rich crystallites containing dislocations, vacancies, stacking faults, and, in some cases, amorphous regions.[26, 70] Once a minimum crystallite size, or comminution limit, is reached, further mechanical input can no longer be efficiently accommodated by fragmentation and is instead stored within the crystal lattice as an increased defect density and internal strain.[69] This stored energy raises the internal free energy of the solid, lowering activation barriers and enhancing reactivity, thereby enabling phase transformations and chemical reactions that are otherwise kinetically inaccessible under ambient conditions.[71] Such defect-mediated mechanical activation has been widely documented across molecular solids, inorganic materials, and metal hydrides, and is increasingly recognised as a key factor governing induction periods, reaction onset, and steady-state behaviour in ball milling systems.[2, 27, 69]

A synchrotron study (Figure 50) highlights the crucial role of the induction period in ball-milling reactions.[55] It uses the 3 part small milling and Fritsch P23 ball mill, the setup at the synchrotron as illustrated in Figure 55.

During NG of an equimolar theophylline (tp)–benzamide (ba) mixture at the BESSY II synchrotron (Berlin), the 1:1 tp:ba Form I cocrystal (blue) emerges only once the crystallite size of tp (green) falls below ~100 nm, despite ba (pink) already being reduced to below 50 nm (Figure 50c).This point is reached at about 600s, marking the end of the induction stage and the start of the sigmoidal reaction stage.[55]

Consistent with this observation, Emmerling et al.[72] reported through synchrotron studies that premilling tp prior to milling under NG conditions with an equimolar amount of commercially available ba significantly reduces the induction period for formation of the 1:1 tp:ba Form I cocrystal. In contrast, premilling ba before addition to commercially available tp has no measurable effect on either the induction period or the overall rate of Form I formation. Density functional theory (DFT) calculations further indicate that tp is the rate-limiting component in Form I cocrystal formation, as it adopts the most stable crystalline state among the reagents. This high lattice stability necessitates preactivation, thereby rationalising the observed acceleration upon premilling tp [72]

View Article Online DOI: 10.1039/D6CP00418B

The role of crystallite size in ball milling-induced tpba Form I → Form II polymorphic transformation was examined, concluding that it depends strongly on solvent type (ethanol, isopropanol, tetrahydrofuran) and loading, with LAG yielding larger sizes than NG. These results indicate that size reduction is not the primary driver of transformation; instead, conversion occurs after an induction period terminating at a characteristic minimum crystallite size of the starting polymorph.[69]

A similar trend was observed in *in situ* synchrotron experiments at BESSY II for the NG metathesis reaction between KI and CsCl, which yields KCl and CsI (Figure 50d–f). The reaction does not commence until both CsCl (green) and KI (violet) have been comminuted to crystallite sizes below approximately 100 nm (Figure 50f).[55]

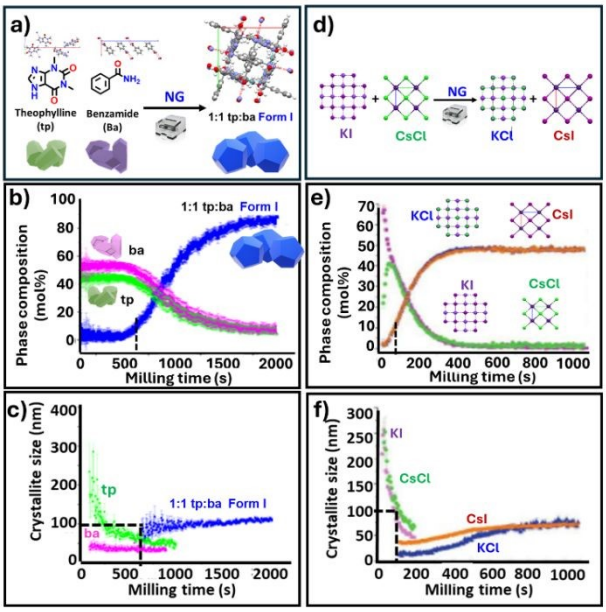

Figure 50 In-situ kinetic profiles measured at the Bessy II synchrotron (Berlin). Left: a) Mechanochemical scheme for formation of 1:1 tp:ba Form I under NG conditions; b) phase-composition kinetics showing consumption of tp and ba and formation of Form I; c) corresponding crystallite-size profile. Right: d) Mechanochemical scheme for the KI–CsCl metathesis under NG conditions, forming KCl and CsI; e) phase-composition kinetics showing consumption of KI and CsCl and formation of KCl and CsI; f) corresponding crystallite-size profile. All profiles show three stages—induction, reaction, and steady-state.[55] Adapted from Ref 55 [https://www.nature.com/articles/s41467-021-26264-1] under CC BY 4.0 license.

16.1 Lessons learned

These synchrotron findings infer that long induction periods in ball milling reactions may reflect the time required for the starting crystalline materials to be broken down to nanoscale dimensions and to store enough energy as defects before the reaction can proceed. This interpretation is consistent with the need for preactivation of highly stable reagents via premilling to shorten the induction period.

17 From macroscopic to microscopic scales

Experimental access to mechanochemical reactions is limited to macroscopic observables (Figure 51a), which represent the cumulative outcome of many elementary events. The molecular-scale processes occurring during mechanical treatment in a ball mill therefore cannot be observed directly (Figure 51b–c).

In ball milling, these elementary events are commonly referred to as local processes, reflecting the strongly heterogeneous distribution of stresses arising from particle–particle and particle–wall contacts in granular media. As a result, ball milling transformations are intrinsically multiscale: macroscopic reaction kinetics emerge from a population of localised events occurring over broad spatial and temporal distributions.

Recent advances in real-time, in situ characterisation techniques have enabled increasingly precise kinetic measurements, supporting the development of models that relate macroscopic reaction progress to microscopic events associated with individual impacts. However, a mechanistic description based solely on molecular-scale considerations remains insufficient; a consistent framework must also describe how these local events collectively drive the global evolution of the system.

Within this context, kinetic models provide a formal framework for describing ball milling transformations, provided that reliable experimental data are available (Figure 51a). While such data may be obtained from ex-situ kinetic experiments;[51-53] in situ synchrotron-based measurements[55] offer enhanced reliability and temporal resolution.

To bridge local processes and global reaction behaviour, Carta and Delogu proposed a kinetic model based on the statistical nature of powder processing in ball mills.[73] In this model, chemical transformations are assumed to occur only within the trapped volume (V_{ra}), defined as the volume of powder mechanically confined during an impact (Fig. 51a,b). Reactions take place exclusively when the mechanical conditions within V_{ra} exceed a threshold impact intensity, referred to as critical loading conditions (CLCs) (Figure 51b). Under CLCs, severe plastic deformation generates fresh interfaces between reactants, enabling forced mixing and mechanochemical reaction.[73]

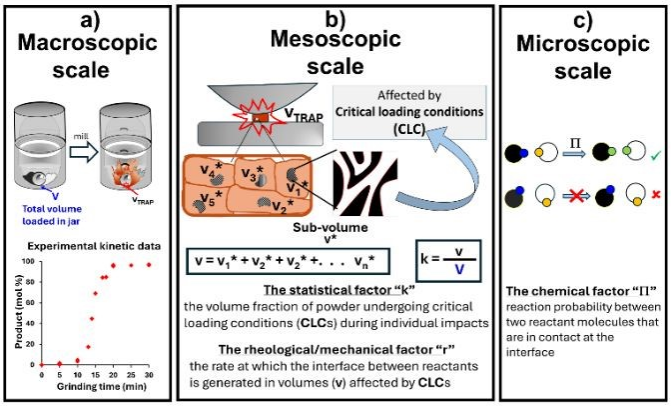

Figure 51 Multiscale view of mechanochemical reactions. a) Macroscopic scale: Powder (V) in the milling jar contains a small, trapped volume (V_{ra}) compressed between the ball and jar. Only global processes are observable. b) Mesoscopic scale: forces in V_{ra} are unevenly distributed, creating sub-volumes (v*). Only regions reaching "critical loading conditions" (CLC) undergo partial transformation, forming new interfaces between reagents (black and white). Parameters k and r are used in the kinetic model.

c) Microscopic scale: Individual molecules react with probability Π, depending on orientation and chemical properties; Π is the third parameter in the kinetic model.[73]

The model relies on three key parameters.

The statistical factor (k) represents the fraction of powder volume experiencing critical loading conditions during individual impacts and reflects the stochastic distribution of powder within the milling jar; it correlates with the slope of the mechanochemical kinetic curve.

The mechanical (or rheological) factor (r) describes the rate at which new reactant–reactant interfaces are generated within volumes subjected to critical loading conditions and thus captures the efficiency of forced mixing at small length scales. Harder solids are associated with lower r values, whereas softer solids yield higher r values.

The chemical factor (Π) represents the probability that two reactant molecules in contact at an interface will undergo chemical reaction, encompassing both thermodynamic driving forces and intrinsic chemical kinetics (Fig.51c).

These parameters are combined into a single mathematical expression that reproduces experimentally obtained mechanochemical kinetic curves.[73] The model is inherently phenomenological and does not enable a priori prediction of reaction outcomes; instead, it requires high-resolution kinetic data obtained under systematic variation of processing parameters, such as:

- Milling frequency[52, 74] (Section 18)
- Milling ball size and density[74, 75] (Section 19)

Despite these limitations, the model provides an effective bridge between macroscopic experimental observables and mechanochemical transformations occurring at mesoscopic and microscopic scales, offering a valuable framework for interpreting and rationalising mechanochemical reactivity.[73]

18 Correlation between milling frequencies and mesoscopic processes

In this section we present two examples, relating the composition at steady-state of the reaction product with the milling frequency: disulfide exchange reaction using 1-2 disulfide system (Section 18.1) and trimerization of $[Ni(dbm)_2]_3$. (Section 18.2).

18.1 Milling frequency on kinetic profiles of disulfide exchange reactions

All experiments on the ball-mill disulfide exchange model reaction (1–2 system) presented in this mini tutorial thus far were conducted using a milling frequency of 30 Hz on an MM400 ball mill. This prompted the question of how reducing the milling frequency would affect the reaction outcome—specifically, whether the mechanochemical reaction would still reach the same steady-state composition observed at 30 Hz.

To address this, kinetic studies were performed on the disulfide 1–2 model system by milling 200 mg powder of equimolar mixture of 1-1 and 2-2 in the presence of DBU with two 7 mm diameter balls for up to 24 h at different frequencies (15, 20, 25, and 30 Hz), under both NG and LAG (50μL MeCN) conditions. The results are summarised in Figure 52.[52]

An exponential relationship was observed between the milling time required to reach steady-state and the milling frequency. This dependence is more pronounced under NG conditions (Figure 52d) than under LAG conditions (Figure 52e). However, macroscopic measurements alone do not allow quantitative determination of these correlations.[52]

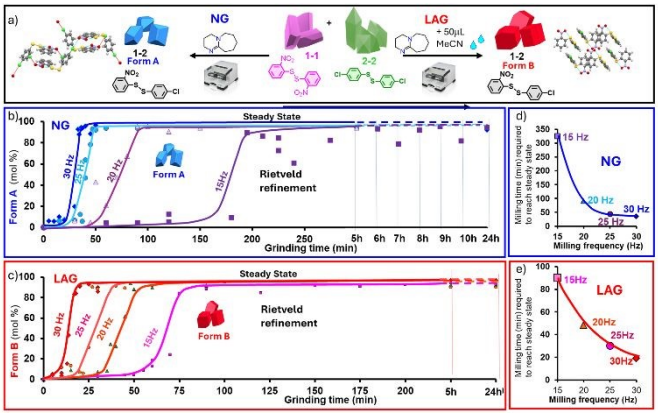

Figure 52 Effect of milling frequency on reaction kinetics of 1-1 + 2-2 with DBU forming 1-2. (a) Reaction scheme. (b) NG kinetics forming only Form A: 15 Hz grinding gives poor mixing and low reproducibility. (c) LAG kinetics (50 μL MeCN) forming only Form B. Each point represents an independent experiment. (d, e) Time to steady-state vs. frequency for NG (d) and LAG (e); lower frequencies require exponentially longer times.[52] Adapted from Ref. [52, DOI: 10.3762/bjoc.15.120], under the terms of the CC BY 4.0 license.

Access to the mesoscopic scale overcomes this limitation and enables the extraction of numerical correlations. Using this approach, phenomenological kinetic equations were fitted to the kinetic profiles obtained at each milling frequency. Notably, a linear relationship was identified between k—defined as the volume fraction of powder experiencing critical loading conditions (CLCs) per unit time—and the cube of the milling frequency (f^3), as shown in Figure 53.[73]

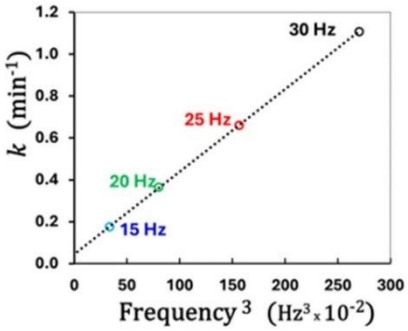

Figure 53) ***k***, the volume fraction of powder effectively affected by CLCs (critical loading conditions) per unit time, as a function of the third power of the milling frequency, f^3. Experiments milled under NG at 15Hz, 20Hz, 25Hz and 30Hz. Data has been taken from the kinetic studies summarised in Figure 52.[52, 73]. Adapted from ref. 73 with permission from [RSC], copyright [2021] and figure drawn with original data supplied by Maria Carta.

18.2 Milling frequency on kinetic profiles of trimerization of brown $(Ni(dbm)_2)$

View Article Online
DOI: 10.1039/D6CP00448B

Another example of the correlation between milling frequency and reaction outcome is illustrated by the ball-mill trimerization of brown bis(dibenzoylmethanato)nickel(II), $Ni(dbm)_2$, to the green trimer $[Ni(dbm)_2]_3$. Ivan Halasz research group uses this model reaction for their mechanistic investigations.[74] This transformation was investigated at four different milling frequencies (27.5, 30, 32.5, and 35 Hz), as summarised in Figure 54.[74]

In these experiments, 200 mg of $Ni(dbm)_2$ was placed in a translucent PMMA vessel (14 mL internal volume) together with a single 8 mm diameter milling ball. Milling was performed using an InSolido Technologies IST635 ball mill at the selected frequencies, and the reaction progress was monitored in situ by Raman spectroscopy.[74]

One kinetic curve was chosen as a reference, and the time axes of the remaining curves were rescaled by a factor ϕ to achieve complete overlap (Figure 54b). This superposition indicates that the chemical transformation proceeds under isokinetic conditions across all four frequencies.[74]

Accordingly, the reaction rate appears to be governed by a single processing parameter, namely, the fraction of powder effectively processed during each impact event. Thus, the scaling factor ϕ can be directly related to k, defined as the volume fraction of powder experiencing critical loading conditions (CLCs) per unit time.

In close analogy with the disulfide exchange system,[73] ϕ was found to scale with the cube of the milling frequency (f^3), as shown in Figure 54b, reinforcing the generality of this mechanistic framework.[74]

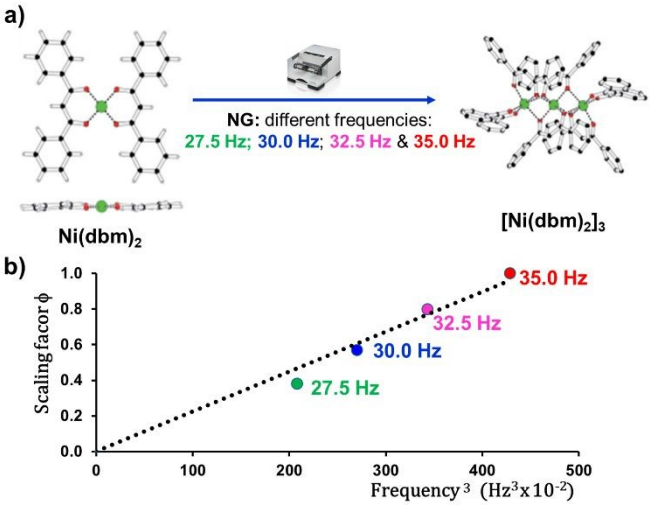

Figure 54 a) Reaction scheme of the trimerisation of brown $(Ni(dbm)_2$ to green trimer, $[Ni(dbm)_2]_3$. b) ϕ, scaling factor, as a function of the third power of the milling frequency, f^3.[74] This is ultimately directly related to $\boldsymbol{k}$ and the volume fraction of powder effectively affected by CLCs (critical loading conditions) per unit time.[74] Adapted from ref. 74 with permission from [RSC], copyright [2022] and figure drawn with original data supplied by Maria Carta.

18.3 Lessons learned

The observed linear relationship between k and f^3 in these two examples highlights the strong dependence of mechanical activation on milling frequency. As the frequency increases, both the number of collisions per unit time and the energy delivered per collision rise, leading to a larger fraction of powder being exposed to critical loading conditions. Consequently, increasing the milling frequency does not merely accelerate the reaction uniformly but increases the probability that powder elements enter mechanically active zones, thereby reducing the time required to reach steady-state.

19 Correlation between the size or density of milling balls and mesoscopic processes

In this section, we present two examples illustrating the correlation between the outcome of NG ball-mill reactions and the milling ball size or ball density at a fixed milling frequency. These examples are the chlorination of *N*-3-ethyl-5,5-dimethylhydantoin in Section 19.1,[75] and the trimerization of brown $Ni(dbm)_2$ in Section 19.2.[74]

19.1 Ball Diameter Effects on Chlorination Kinetics of N-3-Ethyl-5,5-dimethylhydantoin

Figure 55a presents an *in situ* synchrotron-based kinetic study monitored by Raman of the chlorination of N-3-ethyl-5,5-dimethylhydantoin (EDMH) with calcium hypochlorite under NG ball-milling conditions. The reaction was performed using 1 equivalent of EDMH and 2 equivalents of calcium hypochlorite at a total loading of 140 mg and milled at 50 Hz to steady-state to afford 1-chloro-3-ethyl-5,5-dimethylhydantoin (CEDMH). The influence of milling dynamics was investigated by varying the diameter of a single stainless-steel milling ball (2, 4, 5, 6, and 8 mm; Figure 55c).[75]

The results demonstrate that increasing ball diameter improves mixing efficiency (Figure 55b) and leads to an exponential decrease in both the induction period and the time required to reach steady-state (Figure 55d–e).

While macroscopic measurements do not allow direct numerical correlations, the data clearly show that larger and heavier balls promote more efficient reaction progression.

View Article Online
DOI: 10.1039/D6CP00448B

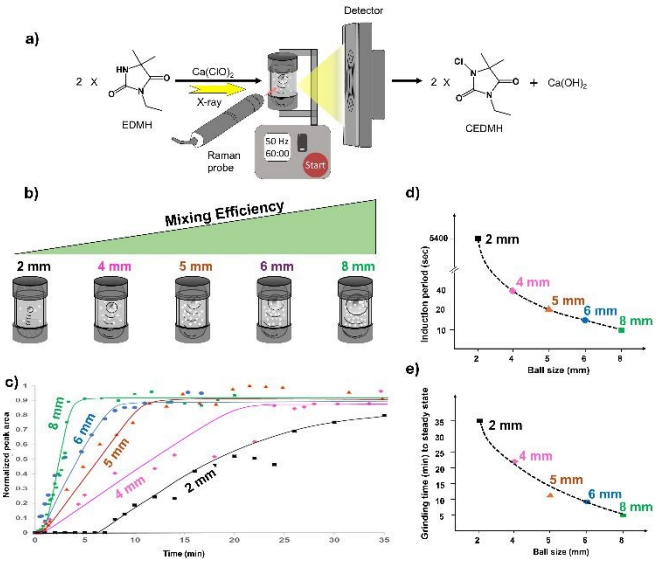

Figure 55 Mechanochemical chlorination of EDMH under NG ball-milling conditions. a) Conversion of EDMH to CEDMH. b) Illustration of enhanced mixing with increasing milling ball diameter. c) Kinetic profiles obtained using a single milling ball (2–8 mm). d, e) Effect of ball diameter on the induction period (d) and time to reach steady-state (e). Graphs d) and e) drawn using original data provided by Ines Martins.[75] Adapted from Ref 75 with permission from *ACS Sustainable Chemistry & Engineering*, 2021, **9**, 12591-12601, Copyright {2021} American Chemical Society.

Application of phenomenological kinetic equations to the kinetic profiles obtained with different ball sizes revealed a linear relationship between k (the volume fraction of powder experiencing critical loading conditions (CLCs) per unit time) and the volume of the milling balls (Figure 56). The physical meaning of k and CLCs is illustrated in Figure 51b, providing a mechanistic interpretation of how ball size governs reaction kinetics.[73, 75]

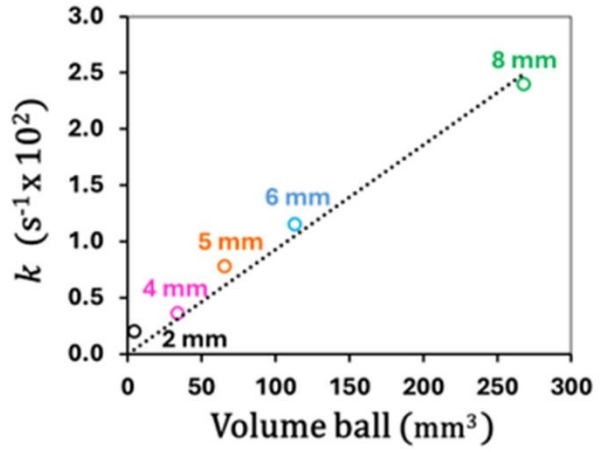

Figure 56 Linear relationship between **k**, the volume fraction of powder effectively affected by critical loading conditions (CLCs) per unit time, and the milling ball volume (2–8 mm diameter). Data based on kinetic studies outlined in Figure 55.[75] Graph drawn using original data provided by Maria Carta. Adapted from Ref 75 with permission from ACS Sustainable Chemistry & Engineering, 2021, 9, 12591-12601, Copyright {2021} American Chemical Society.

19.2 Ball Diameter Effects on Kinetics of trimerization of bis(dibenzoyl-methanato) nickel(II)

Additional insight can be gained by systematically varying the ball density, as illustrated by the ball-mill trimerization of brown bis(dibenzoylmethanato)nickel(II), $Ni(dbm)_2$, to the green trimer $[Ni(dbm)_2]_3$, with the synthetic scheme shown in Figure 58a.[74] The reaction conditions were identical to those described in Section 18.2.[74]

In this study, milling experiments were performed using balls of different masses (8 and 10 mm diameter) fabricated from various materials. Because the reactant and product powders possess distinct mechanical properties, separate kinetic parameters were defined: k_R, corresponding to the fraction of reactant powder experiencing critical loading conditions (CLCs) per unit time, and k_P, describing the fraction of product powder affected per unit time. These parameters reflect the different responses of reactant and product phases to mechanical impacts (Figure 57).[74]

A linear relationship was observed between the fraction of powder processed per single impact and the impact energy E for both k_R and k_P (Figure 57). Extrapolation of these correlations enabled the determination of an activation impact energy, E_o which represents the minimum impact energy required to generate CLCs, i.e., the threshold above which local stresses and shear become sufficient to induce chemical transformation. E_o is correlated to the ball mass in Figure 58).

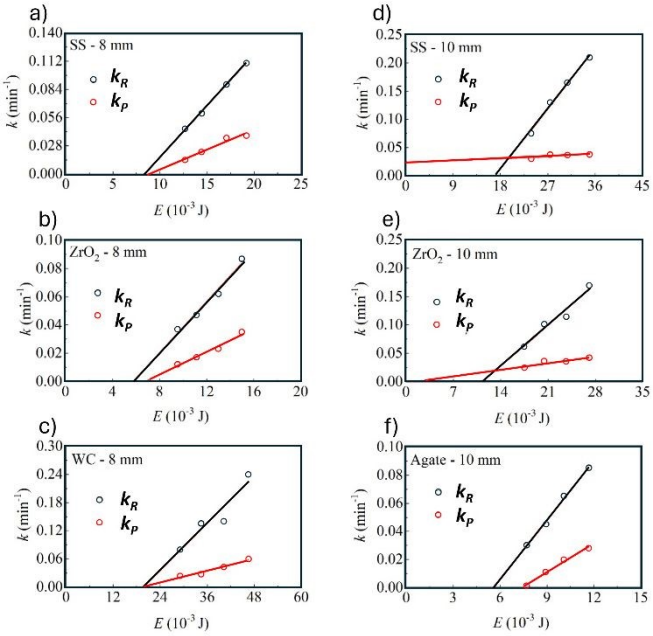

Figure 57: Values of k (the volume fraction of powder experiencing critical loading conditions (CLCs) per unit time) for the reactant phase (k_R) and product phase (k_P) as a function of impact energy *E* in the trimerization of brown $(Ni(dbm)_2$. Left: 8 mm milling balls made of (a) ss, (b) ZrO_2, and (c) WC. Right: 10 mm milling balls made of (d) ss, (e) ZrO_2, and (f) agate. Impact energies *E* were determined through numerical simulations.[74] Adapted from ref. 74 with permission from [RSC], copyright [2022] and figures drawn with original data supplied by Maria Carta.

Furthermore, a linear correlation was established between E_o and the ball mass (m_{ball}) for reactions conducted with 8 mm

View Article Online
DOI: 10.1039/D6CP00448B

balls manufactured with zirconia (ZrO_2, 1.7 g), stainless steel (ss, 2.05 g) and tungsten carbide (WC, 4.1 g) (Figure 58b) and 10 mm balls manufactured with agate (1.3 g), ZrO_2 (3.3 g), and ss (4 g) (Figure 58c). This relationship directly links ball mass to the probability of critical loading conditions (CLC) , reinforcing the mechanistic picture in which mechanochemical reactivity is governed by ball mass, hence the energetic accessibility of mechanically active zones rather than by uniform energy dissipation throughout the powder bed.[74]

This approach allowed the estimation of the activation impact energy, E_o, for each experimental set performed with the same ball type. Furthermore, a linear correlation was determined between the activation impact energy E_o and the ball mass m_{ball} for ball milling reactions conducted with 8 mm (Figure 58b) and 10 mm balls (Figure 58c) made from different materials.[74]

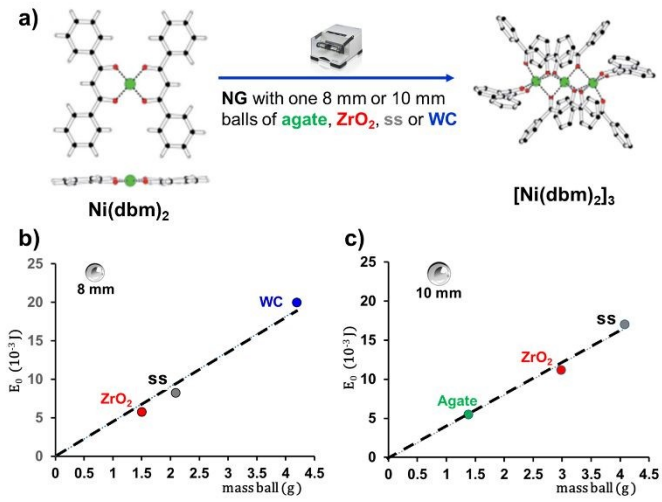

Figure 58 Mechanochemical trimerization of brown ($Ni(dbm)_2$) →green $[Ni(dbm)_2]_3$. a) Reaction scheme. b, c) Activation impact energy (E_o) as a function of milling ball mass (m_{ball}). b) 8 mm balls made from ZrO_2, ss, and WC. c) 10 mm balls made from agate, ZrO_2, and ss. The fraction of reactant powder affected by critical loading conditions per unit time (k_R) correlates directly with E_o.[74] Reproduced from ref. 74 with permission from [RSC], copyright [2022] and figures drawn with original data supplied by Maria Carta.

19.3 Lessons learned

These two published studies suggest that the linear relationship between the impact energy (E_o) and the mass of the milling ball (m_{ball}) could be generally applicable to all mechanochemical reactions.

Conclusions

This mini-tutorial has highlighted how ball milling differs fundamentally from conventional solution-based chemistry by operating under solid-state steady-state conditions governed by relative crystalline stability rather than solution-phase equilibria. As a result, ball milling enables reaction pathways, polymorph selection, and kinetic behaviour that are inaccessible in solution.
Crucially, the outcome of a ball-milling reaction can be reproducibly controlled by a small number of practical parameters, including neat versus liquid-assisted grinding, solvent identity and volume, and by milling to steady-state. These controls allow reliable polymorph interconversion, stabilization of bulk-metastable phases through nanoscale effects, and scalable reaction performance. The concept of steady-state solvent curves provides a simple framework for selecting appropriate LAG conditions and achieving reproducibility and sustainability.
Take-home message: when ball-milling reactions are designed to reach steady-state under well-defined NG or LAG conditions, particularly above the critical solvent volume (V_{100}), reaction outcomes become predictable, reproducible, and recyclable. While the mechanistic details remain largely hidden, the experimentally observable trends presented here offer a practical guide for newcomers and a foundation for future mechanistic and theoretical advances in ball milling.

Author Contributions

This document was written by Ana Belenguer.

Conflicts of interest

There are no conflicts to declare.

Acknowledgements

I am grateful to Professor Jeremy Sanders for his vision and collaboration in exploring ball milling as a discipline requiring fundamental understanding, drawing on his pioneering work in dynamic covalent chemistry (DCC). I thank Giulio Lampronti for his contributions to solid-state analysis and Rietveld refinement, as well as his support in advancing mechanistic understanding of ball milling, and Maria Carta and Francesco Delogu for introducing me to milling dynamics. I further acknowledge Adam Michalchuk, Giulio Lampronti, and Maria Carta for their advice and review of parts of this tutorial, and the reviewers for their valuable suggestions, which improved this minireview tutorial.

References

1. S. L. James, C. J. Adams, C. Bolm, D. Braga, P. Collier, T. Friscic, F. Grepioni, K. D. M. Harris, G. Hyett, W. Jones, A. Krebs, J. Mack, L. Maini, A. G. Orpen, I. P. Parkin, W. C. Shearouse, J. W. Steed and D. C. Waddell, Mechanochemistry: opportunities for new and cleaner synthesis, *Chemical Society Reviews*, 2012, **41**, 413-447.
2. P. Balaz, M. Achimovicova, M. Balaz, P. Billik, Z. Cherkezova-Zheleva, J. M. Criado, F. Delogu, E. Dutkova, E. Gaffet, F. J. Gotor, R. Kumar, I. Mitov, T. Rojac, M. Senna, A. Streletskii and K. Wieczorek-Ciurowa, Hallmarks of

mechanochemistry: from nanoparticles to technology, *Chemical Society Reviews*, 2013, **42**, 7571-7637.

3. K. Tanaka and F. Toda, Solvent-Free Organic Synthesis, *Chem. Rev. (Washington, D. C.)*, 2000, **100**, 1025-1074.
4. L. Takacs, The historical development of mechanochemistry, *Chemical Society Reviews*, 2013, **42**, 7649-7659.
5. O. Galant, G. Cerfeda, A. S. McCalmont, S. L. James, A. Porcheddu, F. Delogu, D. E. Crawford, E. Colacino and S. Spatari, Mechanochemistry Can Reduce Life Cycle Environmental Impacts of Manufacturing Active Pharmaceutical Ingredients, *ACS Sustainable Chemistry & Engineering*, 2022, DOI: 10.1021/acssuschemeng.1c06434.
6. N. Fantozzi, J.-N. Volle, A. Porcheddu, D. Virieux, F. García and E. Colacino, Green metrics in mechanochemistry, *Chemical Society Reviews*, 2023, **52**, 6680-6714.
7. A. A. L. Michalchuk, On the physical processes of mechanochemically induced transformations in molecular solids, *Chemical Communications*, 2024, **60**, 14750-14761.
8. J. F. Reynes, F. Leon and F. García, Mechanochemistry for Organic and Inorganic Synthesis, *ACS Organic & Inorganic Au*, 2024, **4**, 432-470.
9. J. M. Andersen and H. F. Starbuck, Rate and Yield Enhancements in Nucleophilic Aromatic Substitution Reactions via Mechanochemistry, *The Journal of Organic Chemistry*, 2021, **86**, 13983-13989.
10. A. M. Belenguer, G. I. Lampronti, A. J. Cruz-Cabeza, C. A. Hunter and J. K. M. Sanders, Solvation and surface effects on polymorph stabilities at the nanoscale, *Chem. Sci.*, 2016, **7**, 6617-6627.
11. D. Braga and F. Grepioni, Reactions Between or Within Molecular Crystals, *Angewandte Chemie, International Edition in English*, 2004, **43**, 4002-4011.
12. M. R. Ward, C. R. Taylor, M. T. Mulvee, G. I. Lampronti, A. M. Belenguer, J. W. Steed, G. M. Day and I. D. H. Oswald, Pushing Technique Boundaries to Probe Conformational Polymorphism, *Cryst. Growth Des.*, 2023, **23**, 7217-7230.
13. A. M. Belenguer, A. J. Cruz-Cabeza, G. I. Lampronti and J. K. M. Sanders, On the prevalence of smooth polymorphs at the nanoscale: implications for pharmaceuticals, *CrystEngComm*, 2019, **21**, 2203-2211.
14. P. Sacchi, S. E. Wright, P. Neoptolemou, G. I. Lampronti, A. K. Rajagopalan, W. Kras, C. L. Evans, P. Hodgkinson and A. J. Cruz-Cabeza, Crystal size, shape, and conformational changes drive both the disappearance and reappearance of ritonavir polymorphs in the mill, *Proceedings of the National Academy of Sciences of the United States of America*, 2024, **121**, e2319127121.
15. F. Gomollón-Bel, Ten Chemical Innovations That Will Change Our World: IUPAC identifies emerging technologies in Chemistry with potential to make our planet more sustainable.*Journal*, 2019, **41**, 12.
16. S. Sheikhaleslami and J. Sperry, Mechanochemical Radical Transformations in Organic Synthesis, *Chem. Eur. J.*, 2025, **31**, e202403833.
17. A. B. Chetry, Mechanochemistry: A new frontier in chemical synthesis, *Journal of Chemical Research*, 2025, **49**, 17475198251339299.
18. J. M. Marrett, F. Effaty, X. Ottenwaelder and T. Friščić, Mechanochemistry for Metal-Organic Frameworks and Covalent-Organic Frameworks (MOFs, COFs): Methods, Materials, and Mechanisms, *Adv. Mater.*, 2025, DOI: 10.1002/adma.202418707, e2418707.
19. J. J. Zakrzewski, D. Jędrzejowski, J. Wang, H. Tokoro, S.-i. Ohkoshi, D. Matoga and S. Chorazy, Porous Metallophilic Frameworks Incorporating Metal–Organic Chains as Humidity Sensors Exploring Uranyl Photoluminescence, *Advanced Optical Materials*, 2025, **13**, 2403168.
20. Q. Mu and J. Hu, Polymer mechanochemistry: from single molecule to bulk material, *Physical Chemistry Chemical Physics*, 2024, **26**, 679-694.
21. S. Aydonat, A. H. Hergesell, C. L. Seitzinger, R. Lennarz, G. Chang, C. Sievers, J. Meisner, I. Vollmer and R. Göstl, Leveraging mechanochemistry for sustainable polymer degradation, *Polym. J.*, 2024, **56**, 249-268.
22. Y. Xiao, C. Wu, X. Hu, K. Chen, L. Qi, P. Cui, L. Zhou and Q. Yin, Mechanochemical Synthesis of Cocrystal: From Mechanism to Application, *Cryst. Growth Des.*, 2023, **23**, 4680-4700.
23. K. Trzeciak, M. K. Dudek and M. J. Potrzebowski, Mechanochemical Transformations of Pharmaceutical Cocrystals: Polymorphs and Coformer Exchange, *Chem. Eur. J.*, 2024, **30**, e202402683.
24. A. Bose and P. Mal, Mechanochemistry of supramolecules, *Beilstein Journal of Organic Chemistry*, 2019, **15**, 881-900.
25. M. Baláž, *Environmental Mechanochemistry: Recycling Waste into Materials using High-Energy Ball Milling*, Springer, 2022.
26. P. Baláž, *Mechanochemistry in Nanoscience and Minerals Engineering*, Springer, 2008.
27. I. R. Speight, K. J. Ardila-Fierro, J. G. Hernández, F. Emmerling, A. A. L. Michalchuk, F. García, E. Colacino and J. Mack, Ball milling for mechanochemical reactions, *Nature Reviews Methods Primers*, 2025, **5**, 29.
28. D. Margetic, *Organic Mechanochemistry-A New Tool for Sustainable Synthesis*, Elsevier, 2nd edition edn., 2025.
29. A. A. L. Michalchuk, E. V. Boldyreva, A. M. Belenguer, F. Emmerling and V. V. Boldyrev, Tribochemistry, Mechanical Alloying, Mechanochemistry: What is in a Name?, *Frontiers in Chemistry*, 2021, **9**.
30. A. A. L. Michalchuk, in *Mechanochemistry and Emerging Technologies for Sustainable Chemical Manufacturing*, ed. F. G. Evelina Colacino, CRC Press, Boca Raton, 1 edn., 2023, ch. 3, pp. 59-91.
31. R. T. O'Neill and R. Boulatov, The many flavours of mechanochemistry and its plausible conceptual underpinnings, *Nature Reviews Chemistry*, 2021, **5**, 148-167.
32. V. V. Boldyrev, Mechanochemistry and mechanical activation of solids, *Russian Chemical Reviews*, 2006, **75**, 177.
33. S. Karki, T. Friščić, W. Jones and W. D. S. Motherwell, Screening for Pharmaceutical Cocrystal Hydrates via Neat and Liquid-Assisted Grinding, *Molecular Pharmaceutics*, 2007, **4**, 347-354.
34. I. D'Abbrunzo and D. Hasa, More than "just a drop": the enigmatic role of liquid additives in mechanochemistry, *CrystEngComm*, 2026, DOI: 10.1039/D5CE00778J.
35. D. Braga, L. Maini and F. Grepioni, Mechanochemical preparation of co-crystals, *Chemical Society Reviews*, 2013, **42**, 7638-7648.
36. T. Friščić, I. Halasz, P. J. Beldon, A. M. Belenguer, F. Adams, S. A. J. Kimber, V. Honkimäki and R. E. Dinnebier, Real-time

and in situ monitoring of mechanochemical milling reactions, *Nat. Chem.*, 2013, **5**, 66-73.

37. D. Hasa, E. Carlino and W. Jones, Polymer-Assisted Grinding, a Versatile Method for Polymorph Control of Cocrystallization, *Cryst. Growth Des.*, 2016, **16**, 1772-1779.
38. S. A. Salami, M. H. Manyeruke, C. I. Ezekiel, U. N. Ndagano, J. B. Safari, S. O. Amusat and R. W. M. Krause, Recent advances in liquid assisted grinding chemistry: towards sustainable synthesis, *Results in Chemistry*, 2025, **18**, 102675.
39. A. M. Belenguer, G. I. Lampronti and J. K. M. Sanders, Reliable Mechanochemistry: Protocols for Reproducible Outcomes of Neat and Liquid Assisted Ball-mill Grinding Experiments, *JoVE*, 2018, DOI: doi:10.3791/56824, e56824.
40. S. Otto, R. L. E. Furlan and J. K. M. Sanders, Dynamic combinatorial chemistry, *Drug Discovery Today*, 2002, **7**, 117-125.
41. A. M. Belenguer, T. Friscic, G. M. Day and J. K. M. Sanders, Solid-state dynamic combinatorial chemistry: reversibility and thermodynamic product selection in covalent mechanosynthesis, *Chem. Sci.*, 2011, **2**, 696-700.
42. F. Fischer, M. U. Schmidt, S. Greiser and F. Emmerling, The challenging case of the theophylline–benzamide cocrystal, *Acta Crystallographica Section C*, 2016, **72**, 217-224.
43. L. R. K. Snyder, Joseph J.; Glajch, Joseph L. , *Practical HPLC Method Development*, John Wiley & Sons, 2nd edn., 1997.
44. C. R. Groom, I. J. Bruno, M. P. Lightfoot and S. C. Ward, The Cambridge Structural Database, *Acta Crystallographica Section B*, 2016, **72**, 171-179.
45. A. Chapartegui-Arias, A. Raysyan, A. M. Belenguer, C. Jaeger, T. Tchipilov, C. Prinz, C. Abad, S. Beyer, R. J. Schneider and F. Emmerling, Tailored Mobility in a Zeolite Imidazolate Framework (ZIF) Antibody Conjugate, *Chem. Eur. J.*, 2021, **27**, 9414-9421.
46. R. N. Widmer, G. I. Lampronti, S. Anzellini, R. Gaillac, S. Farsang, C. Zhou, A. M. Belenguer, C. W. Wilson, H. Palmer, A. K. Kleppe, M. T. Wharmby, X. Yu, S. M. Cohen, S. G. Telfer, S. A. T. Redfern, F.-X. Coudert, S. G. MacLeod and T. D. Bennett, Pressure promoted low-temperature melting of metal–organic frameworks, *Nat. Mater.*, 2019, **18**, 370-376.
47. J. A. Kaduk, S. J. L. Billinge, R. E. Dinnebier, N. Henderson, I. Madsen, R. Černý, M. Leoni, L. Lutterotti, S. Thakral and D. Chateigner, Powder diffraction, *Nature Reviews Methods Primers*, 2021, **1**, 77.
48. R. E. Dinnebier, A. Leineweber and J. S. O. Evans, *Diffraction Rietveld Refinement: Practical Powder Pattern Analysis using TOPAS*, 2018.
49. S. Lukin, M. Tireli, I. Lončarić, D. Barišić, P. Šket, D. Vrsaljko, M. di Michiel, J. Plavec, K. Užarević and I. Halasz, Mechanochemical carbon–carbon bond formation that proceeds via a cocrystal intermediate, *Chemical Communications*, 2018, **54**, 13216-13219.
50. S. Haferkamp, A. Paul, A. A. L. Michalchuk and F. Emmerling, Unexpected polymorphism during a catalyzed mechanochemical Knoevenagel condensation, *Beilstein Journal of Organic Chemistry*, 2019, **15**, 1141-1148.
51. A. M. Belenguer, G. I. Lampronti, D. J. Wales and J. K. M. Sanders, Direct Observation of Intermediates in a Thermodynamically Controlled Solid-State Dynamic Covalent Reaction, *Journal of the American Chemical Society*, 2014, **136**, 16156-16166.
52. Ana M. Belenguer, A. A. L. Michalchuk, G. I. Lampronti and J. K. M. Sanders, Understanding the unexpected effect of frequency on the kinetics of a covalent reaction under ball-milling conditions, *Beilstein J. Org. Chem.*, 2019, **15**, 1226–1235.
53. A. M. Belenguer, G. I. Lampronti and J. K. M. Sanders, Implications of Thermodynamic Control: Dynamic Equilibrium Under Ball Mill Grinding Conditions, *Israel Journal of Chemistry*, 2021, **61**, 764-773.
54. A. M. Belenguer, A. A. L. Michalchuk, G. I. Lampronti and J. K. M. Sanders, Using Solid Catalysts in Disulfide-Based Dynamic Combinatorial Solution- and Mechanochemistry, *ChemSusChem*, 2022, **15**, e202102416.
55. G. I. Lampronti, A. A. L. Michalchuk, P. P. Mazzeo, A. M. Belenguer, J. K. M. Sanders, A. Bacchi and F. Emmerling, Changing the game of time resolved X-ray diffraction on the mechanochemistry playground by downsizing, *Nature Communications*, 2021, **12**, 6134.
56. A. P. Amrute, Z. Łodziana, H. Schreyer, C. Weidenthaler and F. Schüth, High-surface-area corundum by mechanochemically induced phase transformation of boehmite, *Science*, 2019, **366**, 485-489.
57. I. J. Lin and S. Nadiv, Review of the phase transformation and synthesis of inorganic solids obtained by mechanical treatment (mechanochemical reactions), *Materials Science and Engineering*, 1979, **39**, 193-209.
58. A. Navrotsky, L. Mazeina and J. Majzlan, Size-Driven Structural and Thermodynamic Complexity in Iron Oxides, *Science*, 2008, **319**, 1635-1638.
59. A. Navrotsky, Nanoscale Effects on Thermodynamics and Phase Equilibria in Oxide Systems, *ChemPhysChem*, 2011, **12**, 2207-2215.
60. A. M. Belenguer, G. I. Lampronti, A. A. L. Michalchuk, F. Emmerling and J. K. M. Sanders, Quantitative reversible one pot interconversion of three crystalline polymorphs by ball mill grinding, *CrystEngComm*, 2022, **24**, 4256-4261.
61. M. Descamps, J. F. Willart, E. Dudognon and V. Caron, Transformation of pharmaceutical compounds upon milling and comilling: The role of Tg, *Journal of Pharmaceutical Sciences*, 2007, **96**, 1398-1407.
62. J.-F. Willart, J. Lefebvre, F. Danède, S. Comini, P. Looten and M. Descamps, Polymorphic transformation of the Γ-form of d-sorbitol upon milling: structural and nanostructural analyses, *Solid State Communications*, 2005, **135**, 519-524.
63. N. Bouvart, R.-M. Palix, S. G. Arkhipov, I. A. Tumanov, A. A. L. Michalchuk and E. V. Boldyreva, Polymorphism of chlorpropamide on liquid-assisted mechanical treatment: choice of liquid and type of mechanical treatment matter, *CrystEngComm*, 2018, DOI: 10.1039/C7CE02221B.
64. B. D. Altheimer, S. Pagola, M. Zeller and M. A. Mehta, Mechanochemical Conversions Between Crystalline Polymorphs of a Complex Organic Solid, *Cryst. Growth Des.*, 2013, **13**, 3447-3453.
65. A. A. L. Michalchuk, I. A. Tumanov and E. V. Boldyreva, The effect of ball mass on the mechanochemical transformation of a single-component organic system: anhydrous caffeine, *Journal of Materials Science*, 2018, **53**, 13380-13389.
66. J. P. Mathias, E. E. Simanek, J. A. Zerkowski, C. T. Seto and G. M. Whitesides, Structural Preferences of Hydrogen-Bonded Networks in Organic Solution - the Cyclic

View Article Online
DOI: 10.1039/D6CP00448B

CA3.cntdot.M3 "Rosette", *Journal of the American Chemical Society*, 1994, **116**, 4316-4325.

67. I. C. B. Martins, A. M. Belenguer, G. I. Lampronti and P. Motloch, Three-phase reversible mechanochemical interconversion of hydrogen-bonded melamine : barbiturate co-crystals: from rosette to linear tape polymorphs, *CrystEngComm*, 2025, **27**, 307-310.
68. A. M. Belenguer, G. I. Lampronti, N. De Mitri, M. Driver, C. A. Hunter and J. K. M. Sanders, Understanding the Influence of Surface Solvation and Structure on Polymorph Stability: A Combined Mechanochemical and Theoretical Approach, *Journal of the American Chemical Society*, 2018, **140**, 17051-17059.
69. M. E. Charlesworth, G. I. Lampronti, A. M. Belenguer, S. Day, L. K. Saunders, E. T. Connolly, P. A. Midgley and A. A. L. Michalchuk, Influence of Liquid on Crystallite Size Evolution During Ball Milling, *Cryst. Growth Des.*, 2026, DOI: 10.1021/acs.cgd.5c01662.
70. A. A. L. Michalchuk, The mechanochemical excitation of crystalline LiN3, *Faraday Discussions*, 2023, **241**, 230-249.
71. I. Tole, K. Habermehl-Cwirzen and A. Cwirzen, Mechanochemical activation of natural clay minerals: an alternative to produce sustainable cementitious binders – review, *Mineralogy and Petrology*, 2019, **113**, 449-462.
72. C. Heinekamp, T. M. Palmer, D. Al-Sabbagh, A. May, C. Prinz, S. Michalik, A. A. L. Michalchuk and F. Emmerling, Pre-Activation as a Route for Tuning the Kinetics of Mechanochemical Transformations, *Angewandte Chemie International Edition*, 2026, **65**, e16632.
73. M. Carta, F. Delogu and A. Porcheddu, A phenomenological kinetic equation for mechanochemical reactions involving highly deformable molecular solids, *Physical Chemistry Chemical Physics*, 2021, **23**, 14178-14194.
74. L. Vugrin, M. Carta, S. Lukin, E. Meštrović, F. Delogu and I. Halasz, Mechanochemical reaction kinetics scales linearly with impact energy, *Faraday Discussions*, 2023, **241**, 217-229.
75. I. C. B. Martins, M. Carta, S. Haferkamp, T. Feiler, F. Delogu, E. Colacino and F. Emmerling, Mechanochemical N-Chlorination Reaction of Hydantoin: In Situ Real-Time Kinetic Study by Powder X-ray Diffraction and Raman Spectroscopy, *ACS Sustainable Chemistry & Engineering*, 2021, **9**, 12591-12601.

This is a tutorial review.

View Article Online
DOI: 10.1039/D6CP00448B

It does not require new data. Therefore data availability is not required as all the data presented has been already published in various journals.